Outcrop analogue study of Permocarboniferous geothermal sandstone reservoir formations (northern Upper Rhine Graben, Germany): impact of mineral content, depositional environment and diagenesis on petrophysical properties

Achim Aretz[1*], Kristian Bär[1], Annette E. Götz[2,3], Ingo Sass[1]

[1]Technische Universität Darmstadt, Germany
Institute of Applied Geosciences
[2]Keele University, United Kingdom
School of Physical and Geographical Sciences
[3]Kazan Federal University, Russia

Abstract

The Permocarboniferous siliciclastic formations represent the largest hydrothermal reservoir in the northern Upper Rhine Graben in SW Germany and have so far been investigated in large-scale studies only. The Cenozoic Upper Rhine Graben crosses the Permocarboniferous Saar Nahe Basin, a Variscan intramontane molasse basin. Due to the subsidence in this graben structure, the top of the up to 2 km thick Permocarboniferous is located at a depth of 600 to 2,900 m and is overlain by Tertiary and Quaternary sediments. At this depth, the reservoir temperatures exceed 150 °C, which are sufficient for geothermal electricity generation with binary power plants. To further assess the potential of this geothermal reservoir, detailed information on thermophysical and hydraulic properties of the different lithostratigraphical units and their depositional environment is essential. Here, we present an integrated study of outcrop analogues and drill core material. In total 850 outcrop samples were analysed, measuring porosity, permeability, thermal conductivity and thermal diffusivity. Furthermore, 62 plugs were taken from drillings that encountered or intersected the Permocarboniferous at depths between 1,800 to 2,900 m. Petrographic analysis of 155 thin sections of outcrop samples and samples taken from reservoir depth were conducted to quantify the mineral composition, sorting and rounding of grains and the kind of cementation. Its influence on porosity, permeability, the degree of compaction and illitisation was quantified. Three parameters influencing the reservoir properties of the Permocarboniferous were detected. The strongest and most destructive influence on reservoir quality is related to late diagenetic

processes. An illitic and kaolinitic cementation and impregnation of bitumina document CO_2 rich acidic pore water conditions, which are interpreted as fluids that migrated along a hydraulic contact from an underlying Carboniferous hydrocarbon source rock. Migrating oil and acidic waters led to the dissolution of haematite cements in the lower Permocarboniferous formations. During the Eocene subsidence of the Upper Rhine Graben porosity and permeability of the sandstones of these formations were strongly reduced. The second important influence on reservoir quality is the distinct depositional environment and its influence on early diagenetic processes. In early stage diagenesis the best influence on reservoir properties exhibits a haematite cementation that typically occurs in eolian and fluvial depositional environments. It is characterized by grain covering haematite coatings, which are interpreted to inhibit cementation, compaction and illitisation of pore space during burial and was found in eolian sandstones of the Kreuznach Formation. The third important influence on reservoir quality is the general mineral composition and the quartz content which is the highest in the Kreuznach Formation. Based on the integrated study of depositional environments and diagenetic processes, reservoir properties of the different Permocarboniferous formations within the northern Upper Rhine Graben and their changes with burial depth can be predicted with satisfactory accuracy. This leads to a better understanding of the reservoir quality and enables an appropriate well design for exploration and exploitation of these geothermal resources.

Introduction

The current interest in the geothermal potential of the Upper Rhine Graben makes a detailed assessment of potential target formations for future geothermal reservoir utilization necessary. Data from outcrop analogue studies and from deep boreholes serve as reliable information for reservoir prognosis and are the basis for geothermal field development and well design. Here, we present new petro- and thermophysical data of Permocarboniferous sedimentary series of the northern Upper Rhine Graben and report on the impact of the depositional environment and diagenesis with respect to reservoir quality.

Permocarboniferous siliciclastic deposits consisting of fine-, middle- and coarse-grained sandstones, siltstones, volcanics and subsidiary volcaniclastics and carbonates (Schäfer 2005) presumably represent the largest hydrothermal reservoir in the northern part of the Upper Rhine Graben in SW Germany and

have so far been investigated in large-scale studies only (Haenel and Staroste 1988, 2002, Hurter and Schellschmidt 2003). At its northern end, the Eocene Upper Rhine Graben crosses the Permocarboniferous Saar Nahe Basin, a Variscan intramontane molasse basin. In this area the top of the up to 2 km thick Permocarboniferous is located at a depth between 600 and 2,990 m and covered by Tertiary and Quaternary sediments (Fig. 1). Recently this succession has drawn attention for the evaluation and exploitation of its geothermal potential (e.g., Bär 2008, 2012, Bär et al. 2011, Sass and Hoppe 2011, Rohrer 2010, Wenke et al. 2009, 2011). It is crucial to understand the porosity in the subsurface because it largely determines the thermal properties of sandstones (e.g. Abdulagatova et al. 2009, Clauser and Huenges 1995, Hartmann et al. 2005, Popov et al. 1999) and its matrix permeability (e.g. Pape et al. 1999). The reservoir temperatures of the Permocarboniferous modeled by Arndt et al. (2011) and by Agemar et al. (2012, 2013) for reservoir depth in the northern Upper Rhine Graben exceed 150 °C. Thus, electricity generation with binary geothermal power plants is feasible and deep geothermal energy is already successfully exploited with power generation from plants in comparable settings in the middle Upper Rhine Graben. In Landau, Insheim and Bruchsal the producing reservoirs are fractured crystalline basement rocks, fractured sandstones of the Triassic Buntsandstein and from the Permocarboniferous. The first power plant which will utilize geothermal energy from the siliciclastic and volcanic succession of the Permocarboniferous in the northern Upper Rhine Graben is currently planned in Groß-Gerau (Fig. 1).

Hydrothermal reservoirs

A hydrothermal reservoir suitable for the use of power generation with binary systems should at least have reservoir temperatures of more than 100 °C and permeabilities of more than $1 \cdot 10^{-13}$ m² (e.g. DGG/DGGT 2014). Referring to the fluid transport in hydrothermal reservoirs, the rock permeabilities along fault and fracture systems may be two magnitudes higher than matrix permeabilities (Evans et al. 1997, Lockner et al. 2000, Rawling et al. 2001, Stober and Bucher 2007, Stober and Jodocy 2009). However, high matrix permeabilities of the Buntsandstein in the middle Upper Rhine Graben may contribute with 30 % to the overall fluid transport in fractured reservoir rocks (Bitzer 2007). Bär (2012) and Aretz et al. (2013) investigated bulk rock permeabilities of the Permocarboniferous derived from

hydraulic tests in shallow wells. In the present study, the focus is on the investigation of rock matrix properties and related petrophysical properties and their controlling factors. The effective thickness of the hydrothermal reservoir of the Permocarboniferous as defined in this study is referred to the thickness of sandstone beds with considerable matrix permeabilities of the siliciclastic part and ranges between 200 and 500 m (Schäfer 2005, Schäfer 2011, Becker et al. 2012).

Outcrop analogue studies

The deep geothermal sandstone reservoir of the Permocarboniferous in the northern Upper Rhine Graben is characterized by a small-scale distribution, different orientations and lengths of faults and fractures affecting the properties of the rock matrix, which are controlled by the lithofacies type, porosity and permeability relation and diagenetic history (Henk 1992, Stollhofen 1998, Schäfer 2011,. A broad understanding of these complex interactions as well as the spatial distribution of the structural, sedimentological and diagenetic key elements is usually limited in the subsurface but essential for a reservoir characterization and can only be established by the use of outcrop analogue studies. The advantages of outcrop analogue studies compared to the analysis of core material are the investigation of large-scale sedimentary and structural features, the generation of a representative dataset and the cost-effectiveness. First reservoir modelling on data based on outcrop analogues took place in the 1990s by the Norwegian Oil Companies (Dreyer 1990, Koegh et al. 2014). The most robust match between the analogue and the modelled interval (Howell et al. 2014) is documented for oil fields (Alsop et al. 2013, Pranter et al. 2013) where the actual reservoir crops out next to them. Eschard et al. (2013) built synthetic seismic profiles from their outcrop data in Pakistan to determine which aspects would change under normal subsurface conditions. Furthermore, analogue studies were conducted for eolian depositional systems (e.g. Mountney et al. 1999, Clemmensen 1987) and for fluvial depositional systems (e.g. Fielding and Crane 1987, Gibling 2006, Koegh et al. 2014). For studying structural elements in outcrop analogues today, photogrammetry and LiDAR techniques are used to provide 3D virtual outcrops (Enge et al. 2007, Buckley et al. 2008, Hodgetts 2013) making outcrop analogue studies a well-established method in the exploration industry (Jahn et al. 2008).

In geothermal exploration outcrop analogue studies were applied only recently. Homuth et al. (2014) conducted an outcrop analogue study and comparison of petrophysical data for the assessment of a deep geothermal carbonate reservoir in the Molasse Basin, southern Germany. Petrophysical data of wells were related to petrography and sedimentary facies in the North German Basin by Barth et al. (2014) and in the Thuringian Syncline in Central Germany by Beyer et al. (2014). In the Upper Rhine Graben the two ongoing projects "AuGE" (Outcrop analogue studies for geothermal exploration, Grobe et al. 2013) and "StörTief" ("deep fault zones", Schmidt et al. (2015)) focus on outcrop analogue studies of all potential Mesozoic and Palaeozoic reservoir units. Earlier, the GeotIS project produced a Germany-wide atlas for the description of options for geothermal use (Schulz et al. 2013). The Hessen 3D project first used outcrop data to assess the geothermal potential in the northern Upper Rhine Graben (Bär 2012, Sass and Hoppe 2011, Bär et al. 2011), and the GeORG project investigated the potential of deep reservoirs of the central and southern Upper Rhine Graben (GeORG-Projektteam, 2013).

Limitations of outcrop analogue studies consist in the comparability of petrophysical data from reservoir and its outcrop analogue (Howell et al. 2014) since their degree of weathering, pressure and temperature conditions and diagenetic history affecting these data are completely different for certain time periods. Our study contributes to a better understanding of the petro- and thermophysical properties of siliciclastic rocks of a graben system and the relation between the reservoir and its outcrop analogue with respect to mineral content, depositional environment and diagenetic history.

Geologic setting

By late Variscan (Stephanian-Autunian) wrench tectonics a system of Permocarboniferous troughs and highs was formed (Lützner and Kowalczyk 2012). During Permocarboniferous times the study area was located in peri- and intramontaneous basins in the Variscan mountain belt. With an extension of approximately 100 x 30 km the Saar Nahe Basin is the largest and with a cumulated sediment thickness of 8 km the deepest of about 70 intramontane basins that have been initially formed due to a rift phase causing a long-range extensional regime and the erosion of the Variscan orogen (Hertle 2003, Henk 1992, Henk 1993a, Stollhofen 1998). At the northern border of the Saar Nahe Basin the reactivated NE striking Variscan Hunsrück Taunus Boundary Fault (HTBF) acted as an oblique-normal fault with a

large throw, resulting in a half-graben geometry and a shifting location of the basin depocenter in the northwest following the Variscan NE striking direction (Müller 1996, Schäfer 2011). The initial rift-phase of this half-graben was accompanied by the deposition of claystones, sandstones, conglomerates, limestones and coal beds (Schäfer 1986) with a total thickness of 3,800 to 4,700 m (Stollhofen 1998). Stratigraphically, this period comprises the Carboniferous and the Glan Subgroup as lower part of the Permocarboniferous including the Kusel, Lebach and Tholey beds. With the onset of the Carboniferous basin fill, NE prograding fluvial-deltaic depositional environments caused the deposition of sandstones and mudstones and intercalated coal beds reaching the Frankfurt area (Henk 1993b, Müller 1996). These coals are the source rocks for hydrocarbons.

During the deposition of the 840 m thick Kusel beds (Boy 2005), which form the basal unit of the Permocarboniferous, meandering rivers and lakes were the dominant depositional environments (Müller 1996, Schäfer 1980, Schäfer 2011, Fig. 2). Fluvial deposits show intense oxidation (Füchtbauer 1988, Reading 1996, Miall 1996, Bjørlykke 2010). During the deposition of the 930 m thick Lebach beds (Boy 2005) a narrowing of the Saar Nahe Basin and a higher relief of the source areas caused a change of the fluvial style to rather braided river systems (Schäfer 1980). Due to the continuing depocenter shift along the HTBF in NE direction, the basin extended towards the area of the Wetterau Basin (Kowalczyk 2001). Fluvial deposits with a thickness of up to 800 m are partly correlated with stratigraphic units above the Kusel beds in the Saar Nahe Basin (Marell 1989). In the 360 m thick Tholey beds (Boy 2005) a planation of the basin is recorded, causing the sedimentary regime to change back to a meandering fluvial style. The axis of these meander belts with drainage areas reaching far beyond the basin, was parallel to the Variscan basin axis (Schäfer 2005).

This evolution resulted from a tectonic reorganization of the basin. A NW-SE compression of the Variscan orogen caused a weak folding of the basin and was accompanied by the volcanism of the Donnersberg Formation, which forms the basal unit of the Nahe Subgroup (Upper Permocarboniferous). This formation comprises basaltic and andesitic lava flows, tuffs and pyroclastic deposits with large lateral extend and a maximum thickness of 1,100 m (Stollhofen 1994). These volcanic products are intercalated with coarse-grained siliciclastic deposits. The continuing oblique subsidence at the HTBF

led both to the formation of alluvial fans along the northern basin margin that reach into the basin for several kilometres (Wadern Formation). The circulation of groundwater through these fan deposits caused intense oxidation at least of the upper sediments (e.g. Bjørlykke 2010). It also caused a continuing shift of the depocenter towards NE (Schäfer 1989, Marell 1989) which in turn affected the deposition of up to 250 m thick fluvial and alluvial sediments of the Langen and Moret beds in the Sprendlinger Horst area (Marell 1989, Boy 2005), the stratigraphic equivalents of the Donnersberg Formation of the Saar Nahe Basin (Müller 1996).

The top of the Donnersberg Formation marks the end of the syn-rift phase (Henk 1993b). In the post-rift phase the sedimentation was not controlled tectonically anymore but by thermal subsidence (Stollhofen 1998). The sediment thickness of the Upper Nahe Subgroup amounts to 1,500 m (Stapf 1982). The sedimentation crossed the tectonic borders and even covered the Hunsrück Mountains and the southern source areas. The dominance of eolian and fluvial depositional environments led to the deposition of middle- to coarse-grained sediments of the 260 m thick Kreuznach and 300 m thick Sponheim formations (Boy 2005). Due to decreasing volcanic and tectonic activity as well as a climate shift towards arid conditions, the basin geometry flattened and playa conditions became dominant, leading to the deposition of red siltstones and fine sandstones of the 770 m thick Nierstein Formation in the Saar Nahe Basin (Schwarz et al. 2011) and the 300 m thick Bleichenbach beds in the Wetterau Basin (Kowalczyk 2001). Playa systems formed in depressions under arid conditions which led to the formation of calcitic evaporates as the first member of evaporation cycles. A permanent flow to NW into the North German Basin though inhibited the formation of anhydrites or other evaporites (Ziegler 1990).

The maximum burial depth of the study area is unknown. The primary post-depositional thickness of the Permocarboniferous sediments, which had been eroded from Cretaceous to Tertiary times was studied by Henk (1992) based on the compaction of clay minerals. The calculated overburden in the southwestern part of the Saar Nahe Basin is 1,950 m and in the northeastern part up to 2,450 m. Thus, in the Saar Nahe Basin a maximum burial depth of around 2 to 2.5 km is estimated based on shale compaction (Henk 1992) and vitrinite reflection data (Hertle 2003). In the Mainz Basin east of the Saar Nahe Basin 600 m overburden was eroded (Henk 1992). Angular unconformities reveal that during the

Permian, from the Buntsandstein until the Jurassic and from the Eocene until the Lower Miocene erosion events took place.

In the Oligocene a Trans-European rift system developed between the Mediterranean and the North Sea (Illies 1972, Behrmann et al. 2005, Walter and Dorn 2007), the 300 km long and up to 40 km wide N-S trending Upper Rhine Graben representing its largest part. Its subsidence led to a vertical fault throw of up to 4.5 km and resulted in an increased geothermal gradient by the upwelling of hot fluids from the fractured upper crust (Teichmüller and Teichmüller 1979, Clauser and Villinger 1990, Pribnow and Schellschmidt 2000). At the northern end of the Upper Rhine Graben the top of the 2 km thick Permocarboniferous is located at depths between 600 and 2,990 m (Müller 1996, Schäfer 2005, Becker et al. 2012). With an area of about 1,000 km² the Permocarboniferous siliciclastic formations represent the largest hydrothermal reservoir with temperatures of more than 150°C in the northern Upper Rhine Graben (Arndt et al. 2011, Bär et al. 2011, Sass and Hoppe 2011, Bär 2012, Aretz et al. 2013).

Materials and methods

In the present study, outcrop analogue studies have been conducted in the Saar Nahe Basin, the Sprendlinger Horst and in the Wetterau Basin west and east of the northern Upper Rhine Graben (Fig. 3) to gain a new dataset of petro- and thermophysical rock properties.

Sampled outcrops include mainly active and abandoned quarries and additionally road cuts and natural scarp slopes. Depending on the outcrop conditions, a detailed sedimentological analysis was conducted. Macro- to mesoscopic sedimentary structures of the outcrop, including layer thickness, horizontal and vertical sequences of beds were described as well as internal bedding structures such as ripple marks, cross bedding and erosional surfaces, internal grading and sorting and intercalations. Finally, together with the colour and grain size of the individual beds, all these observations were used to detect the type of the predominant depositional environments including playa, eolian, alluvial, lacustrine, meandering fluvial and braided fluvial systems according to classifications of Füchtbauer (1988), Miall (1996), Reading (1966) and Bjørlykke (2010).

In the Saar Nahe Basin 686 samples were taken from 71 outcrops. Additionally, one drill core with depths from 10 to 70 meters was sampled. In the Sprendlinger Horst 94 samples were taken from 4 outcrops and two drill cores with depths from 0 to 55 and 65 meters respectively were sampled. In the Wetterau Basin 43 samples were taken from 5 outcrops. Additionally, 62 plugs were sampled from drill cores of the 6 hydrocarbon exploration wells Worms 3, Nordheim 1, Gimbsheim 2, Stockstadt 33R, Weiterstadt 1 and Königstätten 3. These wells intersected the Permocarboniferous in the northern Upper Rhine Graben at depths of 1,550 to 2,900 m. Each of the identified 14 lithostratigraphic units and six depositional environments including fluvial braided and meandering, lacustrine, alluvial, eolian and playa settings were sampled.

The rock samples were cut to cylindrical plugs with lengths of 20 to 30 mm and diameters of 40 mm. They are orientated either parallel or orthogonal to bedding and were oven dried at 105 °C for at least 24 hours. The petro- and thermophysical parameters measured include porosity, permeability, density, thermal conductivity and thermal diffusivity. Petrographic analyses include mineral composition, sorting and rounding of grains, the kind of cementation and the determination of cementation types. These analyses complement the macroscopic outcrop analyses, enabling the identification of distinct depositional environments.

The porosity was measured with the helium pycnometer AccyPyc 1330 (micromeritics) and the bulk (or raw) density with the powder pycnometer GeoPyc 1360 (micromeritics). For the determination of the matrix permeability a columnar gas permeameter was used (Filomena et al. 2014). The apparent permeability is measured at five different pressure stages from 1 to 5 bar to enable the calculation of the intrinsic permeability (Klinkenberg 1941). The thermal conductivity and diffusivity was measured with an optical thermal scanner (Lippmann and Rauen 2005). The measurement is based on the optical scanning method after Popov et al. (1999). The measurement methods do not consider reservoir temperature, pressure and fluid properties. Samples are therefore measured oven-dry to enable comparability and improving accuracy. A tool for the prognosis of geothermal reservoir properties of deep sedimentary basins and graben settings is the thermofacies concept introduced by Sass and Götz (2012) who showed that permeability and thermal conductivity, significantly responsible for the heat

flow, are depending on the distinct lithofacies type. In the present study, the petro- and thermophysical data from outcrops and boreholes were evaluated in terms of depositional environments.

For petrographic analyses one thin section per sampling locality was prepared. In total 120 thin sections of outcrop and shallow borehole samples and 35 thin sections of samples taken from reservoir depth were examined. The mineral composition was studied by pointcounting of at least 300 grains per sample. The sorting and rounding and the kind of cementation were studied and porosity was pointcounted according to Paxton et al. (2002). Since diagenetic processes have a strong influence on the evolution of porosity and permeability with burial (Gaupp 1996, Molenaar 1998, Wolfgramm 2005) the influence of different cementations and depositional environments on porosity and permeability, degree of compaction (Houseknecht, 1988), and illitisation of pore space were investigated.

Results

Sandstone petrography and depositional environments

Six depositional environments including playa, eolian, alluvial, lacustrine, fluvial braided and meandering settings were identified in the Permocarboniferous outcrops studied (Fig. 4):

(1) Sandstones of playa depositional systems have a dark red colour, are fine laminated and exhibit small-scale cross-bedding structures in outcrops (Fig. 4.A1). These sandstones are very poorly to poorly sorted with grain sizes ranging from silt to fine-grained sand (Fig. 4.A2, 4.A3) showing a high feldspar content (Fig. 5a).

(2) Sandstones of eolian depositional systems are characterized by a red colour and up to 3 to 5 meter thick cross-bedding structures in outcrops (Fig. 4.B1). They have rounded to well-rounded and well to very well-sorted grains with middle to coarse grain sizes and high porosities (Fig. 4.B2). In outcrops, eolian sandstones show a high amount of rock fragments (Fig. 5a), in the reservoir they are quartz-rich (Fig. 5b).

(4) Sandstones deposited in alluvial depositional systems exhibit a grey and reddish colour in outcrops and show a characteristic stacking pattern of small-scale, 15 to 40 cm thick fining-upward cycles. The

base of the cycles is marked by up to 5 cm long angular rock fragments, the top features middle sand size (Fig. 4.C1) which we interpreted as proximal fan deposits. Alluvial sandstones are poorly sorted with grain sizes from fine-grained sand to gravel (Fig. 4.C2). In outcrops, alluvial sandstones show a high amount of rock fragments (Fig. 5a), in the reservoir they are enriched in feldspar (Fig. 5b).

(5) Sandstones of lacustrine depositional systems are characterized by millimetre thick laminations of silt and fine-grained sand (Fig. 4.D1, Fig. 4.D2, Fig. 4.D3), partly rich in organic matter and plant fragments or micas at the bedding surfaces. Lacustrine sandstones in the reservoir are enriched in feldspar and mica (Fig. 5b).

(5+6) Sandstones of fluvial depositional systems are characterized by grey and reddish colours in outcrops, cross-bedding structures and ripple marks (Fig. 4.E1, F1). Outcrops of braided fluvial sandstones exhibit thick beds of coarse-grained sandstones (Fig. 4.E1). Braided fluvial sandstones show subangular to subrounded and very poorly to moderately sorted grains with middle to coarse grain sizes (Fig. 4.E2, Fig. 4.E3). Outcrops of meandering fluvial sandstones exhibit alternating beds of coarse-grained and fine-grained sandstones and intercalated thin silt and mudstone beds (Fig. 4.F1). Meandering fluvial sandstones consist of fine sand grains including rock fragments, feldspar and mica (Fig. 4.F3). Fluvial sandstones in the reservoir exhibit higher feldspar contents than those from outcrops (Fig. 5a, b).

Cementation types

The following cementation types were identified in samples taken from outcrops and reservoir depth. In general, cementation types are not restricted to certain depositional environments.

(1) Carbonate cements are pore filling and occur as carbonate crystals (Fig. 4.C3) with high interference colours or dolomitic crystals with low interference colours. Sampled sandstones with calcitic cements are summarized as C-type sandstones and with dolomitic cement as D-type sandstones, respectively.

(2) Illitic palates exhibit sizes of less than 5 micrometres. Their growth is restricted on the surface of grains (Fig 4.E2). Sampled sandstones with illitic palates covering grain surfaces are summarized as I-type sandstones.

(3) Haematite cement is characterized by 5 to 20 micrometre thick aggregates of opaque to reddish and brown coatings covering grain surfaces (Fig. 4.B2, van Houten 1973, Gaupp 1996, Schöner 2006). Sampled sandstones with haematite cement are summarized as H-type sandstones.

(4) Pore filling illitic cement consists of illite crystals at pore necks that grow into the pore space and may fill it completely (Fig 4.F3). Sandstones with pore filling illitic cement are summarized as IL-type sandstones.

(5) Kaolinitic cement consists of small kaolinitic crystals in the pore space (Fig 4.F2). Sandstones with kaolinitic cements are summarized as K-type sandstones.

(6) Bitumina cement is a pore filling opaque black cement (Fig. 4.F2). Sandstones with bitumina impregnations are summarized as B-type sandstones.

Petro- and thermophysical parameters of the stratigraphic units

The highest porosities and permeabilities occur in outcrops of the Thallichtenberg Formation's Tholey beds with 19.1 % and $1.4 \cdot 10^{-15}$ m², the Remigiusberg Formation's Kusel beds with 16.4 % and $3.8 \cdot 10^{-15}$ m², and the Kreuznach Formation of the Nahe Subgroup with 16.3 % and $2.9 \cdot 10^{-15}$ m² (Table 1a). The highest thermal conductivities and diffusivities of outcrop samples exhibit the Quirnbach Formation with 2.78 $Wm^{-1}k^{-1}$ and $1.62 \cdot 10^{-6}$ m²/s, the Wadern Formation with 2.59 $W/m^{-1}k^{-1}$ and $1.76 \cdot 10^{-6}$ m²/s, and the Langen Formation of the Sprendlinger Horst with 2.61 $Wm^{-1}k^{-1}$ and $1.54 \cdot 10^{-6}$ m²/s.

Samples taken from reservoir depth exhibit the highest porosities and permeabilities in the Kreuznach Formation with 14.0 % and $1.6 \cdot 10^{-15}$ m² and in the Wadern Formation with 8.5 % and $4.9 \cdot 10^{-15}$ m² (Table 1b). The highest thermal conductivities were measured on samples from the Lauterecken Formation with 2.92 $Wm^{-1}k^{-1}$ and on samples from the Disibodenberg Formation with 2.88 $Wm^{-1}k^{-1}$; the

highest thermal diffusivities were obtained from the Nierstein Formation with $1.65 \cdot 10^{-6}$ m²/s and the Kreuznach Formation with $1.59 \cdot 10^{-6}$ m²/s.

Regarding the petrographic composition of the outcrop samples, the Wahnwegen Formation has the highest quartz content with 68.1 % (Table 2a). The highest feldspar content occurs in the Quirnbach Formation with 25.4 %, the highest content of lithic fragments in the Sponheim Formation with 76.4 % and the highest mica content in the Altenglan Formation with 15.5 %. The highest intergranular porosity was found in samples from the Remigiusberg Formation with 18.6 %, the Wahnwegen Formation with 16.3 %, the Langen beds with 13.7 %, and the Kreuznach Formation with 13.2 %.

Samples taken from reservoir depth exhibit the highest quartz content (73.8 %) in the Kreuznach Formation, the highest feldspar content (51.5 %) in the Jeckenbach Formation, the highest content of lithic fragments (34.9 %) in the Wadern Formation, and the highest mica content (28.6 %) in the Odernheim Formation (Table 2b). The Kreuznach and Wadern formations have the highest intergranular porosities with 20.0 % and 14.3 %, respectively.

Petro- and thermophysical parameters of depositional environments

In terms of depositional environments, outcrop samples of eolian sandstones have the highest mean porosities (16.4 %) and the highest mean permeabilities ($2.0 \cdot 10^{-15}$ m²) (Fig. 6a). Sandstones deposited in fluvial meandering systems exhibit mean porosities of 16.1 % and lower mean permeabilities of $7.6 \cdot 10^{-16}$ m², compared to eolian sandstones. The lowest values were identified for lacustrine sandstones with a mean porosity of 4.2 % and a mean permeability of $1.0 \cdot 10^{-18}$ m².

Of the reservoir rocks, the eolian sandstones also exhibit the highest porosities with 12.3 % and the highest permeabilities with $8.4 \cdot 10^{-16}$ m² (Fig. 6b). Both, the sandstones deposited in a fluvial meandering setting and those deposited in a fluvial braided setting are characterized by low porosities of 2.7 % and 2.5 % and permeabilities of $6.1 \cdot 10^{-18}$ m² and $3.2 \cdot 10^{-18}$ m², respectively. The thermal conductivities range between those of eolian sandstones with 2.06 $Wm^{-1}K^{-1}$ and lacustrine sandstones with 2.56 $Wm^{-1}K^{-1}$.

Correlation of cementation types and petrophysical properties

The permeability-porosity plot of the cementation types of outcrop samples (Fig. 7a) illustrates low porosities and permeabilities of C-type sandstones (9.5 %; $6.2 \cdot 10^{-17}$ m²) and of I-type sandstones (5.3 %; $1.3 \cdot 10^{-17}$ m²). For D-type sandstones low porosities and high permeabilities were observed (7.2 %; $2.6 \cdot 10^{-15}$ m²). H-type sandstones show a linear trend of porosity and permeability (16.3 %; $3.2 \cdot 10^{-15}$ m²), which follows the general trend for different comparable sandstones according to Pape et al. (1999). Among the H-type sandstones, those deposited under playa conditions exhibit lower porosities compared to those deposited under eolian conditions (Fig. 7a, b). IL-type and B-type sandstones show similar mean porosity and permeability values (15.5 %; $4.1 \cdot 10^{-16}$ m² and 16.5 %; $5.4 \cdot 10^{-16}$ m²). K-type sandstones exhibit high porosities and permeabilites (18.8 %; $1.6 \cdot 10^{-14}$ m²). The permeability-porosity plot of the dominant cementation types of samples taken from reservoir depth reveals low porosities and permeabilities of C-type sandstones (4.6 %; $1.7 \cdot 10^{-17}$ m²), I-type sandstones (1.8 %; $1.4 \cdot 10^{-18}$ m²), D-type sandstones (0.6 %; $1 \cdot 10^{-18}$ m²), IL-type sandstones (5.3 %; $1.5 \cdot 10^{-17}$ m²), and B-type sandstones (0.6 %; $1.0 \cdot 10^{-18}$ m², Fig. 7c). The H-type sandstones are the only ones showing considerably higher values and a linear trend of porosity and permeability (12.3 %; $2.5 \cdot 10^{-15}$ m²), whilst alluvial H-type sandstones have lower porosities than eolian H-type sandstones (Fig. 7c, d).

Degree of compaction

The intergranular volume (IGV) (Houseknecht 1988, Paxton et al. 2002) can be used to quantify the degree of compaction of sandstones which strongly influences their porosity and permeability (Houseknecht 1987, Houesknecht 1988). The mechanical compaction caused by lithostatic overburden pressures during burial leads to the reorientation and repacking of grains and to the reduction of the bulk volume, which is characterized entirely by the reduction of the IGV (Houseknecht 1987).

The reduction of the IGV caused by mechanical compaction from the initial 40 % assumed for well-sorted and rounded loose sand is limited to 26 % characterizing the arrangement of an ideal sphere packing (Houseknecht 1987). For poorer sorted sandstones with angular or subangular grains, as represented by the rather proximal to medial sandstones sampled in the present study, these values

proposed by Houseknecht (1987) need to be reduced. The IGV can be further reduced only by chemical compaction (grain dissolution) of framework grains at point contacts. This is characterized by intergranular pressure solution and indicates deeper burial depths.

Within the outcrop samples, H-type sandstones exhibit the highest IGVs between 20 and 39 %, and intergranular porosities between 5 and 19 % (Fig. 8a). Of the H-type sandstones, only the eolian sandstones exhibit IGVs above 26 % (Fig. 8a, b). B-type sandstones exhibit IGVs of 12 to 30 %, and intergranular porosities of 8 to 24 %. The IL-type sandstones display lower IGVs of 17 to 26 % and lower porosities of 3 to 10 %. The C-type sandstones are characterized by IGVs between 8 and 34 % and low porosities of up to 6 %. Similar low porosities were observed for the D-type and I-type sandstones. In case of the samples taken from reservoir depth, H-type sandstones also have the highest IGVs between 20 and 40 %, and the highest intergranular porosities of up to 25 % (Fig. 8c). As observed for outcrop samples, of the reservoir samples, the Eolian H-type sandstones exhibit higher intergranular porosities than alluvial H-type sandstones as well (Fig. 8c, d). All samples with other cementation types are characterized by porosities below 2 % whilst the C-type and D-type sandstones display slightly higher IGVs than the IL-type, I-type and B-type sandstones.

Illitisation of pore space

Illitisation strongly reduces the permeability in reservoir sandstones (Bjørlykke 1996, Rossi et al. 2002, Worden and Morad 2003). Since the degree of illitisation is linked directly to the feldspar content, it significantly influences reservoir quality (Rossi et al. 2002).

Among the samples taken from outcrops, the pore filling cements of IL-type sandstones consist of up to 51 % of illite with increasing feldspar content in the modal composition (Fig. 9a). The highest illite content exhibit the cements of I-type sandstones with up to 82 %. The illite content of cements of B-type sandstones amounts up to 30 %. Pore fillings of C- and D-type sandstones exhibit minor illite contents of mostly less than 20 %, despite feldspar contents of up to 37 %. Cements of H-type sandstones exhibit the lowest illite content in the pore space with less than 18 %. Among those, the H-type sandstones deposited under playa conditions exhibit no pore filling illite, despite feldspar contents of up

to 42 % (Fig. 9b). Eolian H-type sandstones exclusively exhibit illite contents in the cements of less than 10 % (Fig. 9a, b).

Among the samples taken from reservoir depth, the cements of the IL-type sandstones exhibit illite contents of up to 79 % (Fig. 9c). Pore fillings of C- and D-type sandstones exhibit minor illite contents of less than 10 %, with feldspar contents in the modal composition of more than 40 %. Among the H-type sandstones, those deposited in eolian environments are the only ones with illite contents of less than 9 % (Fig. 9d).

Correlation of cementation types and lithostratigraphic units

A key finding of our investigations is that both, outcrop samples and reservoir samples of the same stratigraphic units have either been defined as H-cementation type or as IL- /B-cementation types. B- and IL-type sandstones (Fig. 10) characterize the entire Glan Subgroup and the Donnersberg Formation of the Nahe Subgroup. Besides the occurrence of K-type sandstones in the Wadern Formation, the H-cementation type is dominant in the Wadern, Sponheim and Kreuznach formations of the Saar Nahe Basin and the stratigraphic units of the Sprendlinger Horst and Wetterau Basin, respectively. C-, D- and I-type cementations occur irregularly in the entire Permocarboniferous succession.

Discussion

The results suggest a time sequence of the formation of the different cementation types. The C- and D-type sandstones (Fig. 4C3) which exhibit low illite contents despite enhanced feldspar contents (Fig. 9) can be interpreted to have formed during the early diagenesis before the infiltration of clay minerals (Velde 1995, Worden and Morad 2003) which is connected with the formation of the I- and H-type sandstone (Fig. 11). According to Morad (1998) carbonate cement is formed under high salinar pore waters very early in eodiagenesis. According to van Houten (1973), Hasner (2004) and Gaupp (1996) haematite is formed e due to the alteration of instable iron-rich minerals such as pyroxene, hornblende, biotite and heavy minerals during the infiltration of clay minerals. Under oxidizing conditions precipitation of iron takes place in form of iron hydroxides (Fe(OH)3) whose Fe3+ ions are absorbed at the negative charged mud mineral surfaces as ferrihydrite (5Fe2O3 + 9H2O) and goethite (αFeOOH)

(Langmuir, 1997; Scheffer und Schachtschabel, 1992; Turner, 1980; Stumm, 1992). Haematite if formed due to the substitution of ferrihydrite and goethite during dehydration (van Houten, 1973; Metcalfe et al., 1994, Weibel 1999). The syntaxial coatings of haematite occur due to a vertical growth of bigger crystals of up to a few 10er micrometres to the grain surface (Turner, 1980).

Furthermore our data show that sandstones either exhibit H-type or IL- K- and B-types, suggesting that the H-type has been dissolved and replaced by them (Fig. 11).

For iron oxide reduction and bleaching of red sandstones liquid hydrocarbons are considered to be the most reducing agents (Garden et al. 2001, Parry et al. 2004, Schöner 2006). Bleaching of red sandstones often occurs close to faults and fracture zones that acted as conduits for the transport of acidic fluids (Foxford et al. 1996, Beitler et al. 2003, Schöner 2006). There are a number of possible processes that can lead to the reduction of haematite in CO_2-contaminated pore waters. Typical chemical reactions for the reduction of haematite are as follows (Chan et al. 2000):

For hydrocarbons:

$$CH_2O + 2Fe_2O_3 + 8H^+ > CO_2 + 5H_2O + 4Fe^{2+}$$

$$CH_4 + 4Fe_2O_3 + 16H^+ = 10H_2O + CO_2 + 8Fe^{2+}$$

For organic acids:

$$CH_3COOH + 4Fe_2O_3 + 16H^+ > 2CO_2 + 8Fe^{2+} + 10H_20$$

The IL-, K- and B-type are interpretated as being formed due to late diagenetic organic processes (Fig. 11). The IL-type is formed in acidic/CO_2-bearing pore waters when the appropriate pore fluids like K^+ ions are available that may have been provided by kalifeldspar dissolution (Surdam et al. 1984, Gaupp et al. 1993, Cookenboo and Bustin 1999, Barcley and Worden 2000). The K-type is formed in CO_2-bearing pore waters due to the dissolution of kalifeldspar (Emery et al. 1993, Worden and Barcley 2000) in deeply buried sandstones in the vicinity of stratigraphic or structural borders to hydrocarbon source rocks (Gaupp 1996). The B-Type is interpreted as former oil fill (Gaupp 1996, Schöner 2006) that migrated from underlying organic-rich source rocks as for example Carboniferous coal seams (Littke et al. 1996) or oil reservoir rocks in the Upper Rhine Graben (Plein 1993). The strongest and most destructive influence on reservoir quality is related to late diagenetic processes.

According to Worden and Morad (2003), clay reactions slow down after oil migration in a water-wet sandstone and completely stop in an oil-wet sandstone. In the North German Basin Gaupp (1996), Grötsch and Gaupp (2011) and Schöner (2006) have outlined the importance of organic maturation and migration in Permocarboniferous reservoir sandstones. They postulated that the bleaching of sandstones, the illite formation and the bitumen impregnation are closely connected to each other and happen successively.

Our data show that outcrop and reservoir samples of H-type sandstones exhibit the highest porosities and permeabilities (Fig. 7a, c), the highest intergranular volume (Fig. 8a, c), and the lowest illite content in the pore space (Fig. 9a, c). Hence, the H-type can be interpreted as protection against compaction and illitisation during burial. Since the H-type mainly forms in eolian depositional environments (Gaupp 1996, Schöner 2006), increased porosities and permeabilities of eolian reservoir sandstones (Fig. 6b) are expected. The second important influence on reservoir quality is therefore the distinct depositional environment, its influence on early diagenetic processes and formation of haematite cementations that typically occurs in eolian and fluvial depositional environments.

The observation that sandstones from outcrops and reservoir depth of the Glan Subgroup and Donnersberg Formation exhibit IL- and B-type sandstones and almost no H-type sandstones, suggests a migration of liquid hydrocarbons from underyling Carboniferous source rocks or of other CO_2 or CH_4 rich fluids into these formations causing a bleaching of sandstones. Going beyond the assumption of Schöner (2006) that bleaching is limited to the vicinity of faults, we suggest a basin-wide migration that happened either through the matrix as migration of oil or as a progressive bleaching front moving laterally from the faults with time. In the overlying Wadern, Sponheim and Kreuznach formations and in the formations of the Sprendlinger Horst and Wetterau Basin, the occurrence of H-type sandstones suggests that these formations were not contaminated by the occurrence of liquid hydrocarbons. Possible reasons for their absence could be a too large vertical distance from the underyling Carboniferous source rocks since the thickness of the Glan Subgroup and Donnersberg Formation amounts approx. to 3,200 m (Fig. 2, Stollhofen 1998, Boy 2005). Also the lateral pinging out of the Carboniferous towards the East westward of the Sprendlinger Horst might be a reason (Müller 1996). Another reason might be the

termination of the syn-rift phase and the beginning of the post rift-phase at the transition of the Donnersberg, Wadern and Sponheim formations (Henk 1993a), leading to the termination of synsedimentary fault zones and thus absence of conduits for hydrocarbons or CO_2 rich fluids (Fig. 11). Another reason might be the hundreds of meter thick volcanic deposits of the Donnersberg Formation (Stollhofen 1998) that could have acted as a barrier for the migrating hydrocarbon fluids. The observation that in the formations of the Sprendlinger Horst and the Wetterau Basin east of the graben the H-type sandstone is dominant, suggests an absence of hydrocarbon or CO_2 rich fluids since underlying Carboniferous sediments are missing. According to Müller (1996) the occurrence of Carboniferous deposits ended westward of the Sprendlinger Horst (Fig. 1).

Due to the post-Permocarboniferous erosion processes and loss of up to 2.5 km thickness (Henk 1992), the remaining Permocarboniferous succession, which underwent subsidence by at least these amounts, was uplifted and present outcropping sandstones were exposed to telodiagenetic processes where formation waters are replaced by meteoric waters (Worden and Morad 2003). The reducing pressure conditions during the uplift and telodiagenetic processes could have caused a decompaction of the Permocarboniferous sandstones, leading to higher intergranular volumes and increasing matrix porosities and permeabilities of outcrop B-, K- and IL-type sandstones. This effect has always to be kept in mind when conducting outcrop analogue studies to determine petrophysical parameters. In the study presented here, the availability of reservoir samples from deep wells at different depths, which enable direct measurements of petrophysical properties, enables to directly check this effect. Thus, our dataset would allow for a depth dependent prediction of those properties considering the cementation types and depositional environment.

Later, during Eocene times the subsidence of the Upper Rhine Graben affected at its northern end the Permocarboniferous succession (Teichmüller and Teichmüller 1997), leading to a second phase of burial and diagenesis. Only H-type sandstones which formed during the first diagenesis phase kept their haematite coatings as a protection against cementation, further compaction and illitisation and preserved their high porosities and permeabilities at greater depth. In contrast, the B-, K- and IL-type sandstones, which had lost this protection during the first diagenesis phase were strongly reduced in porosity and

permeability. The low porosities and permeabilities of C-, D- and I-type sandstones observed from outcrops were even more reduced during the second diagenesis phase.

This leads to the assumption that the reservoir properties of the Permocarboniferous are primarily dependent on the primary diagenetic processes during Permian times, which strongly influenced those processes that are connected with the Eocene subsidence of the Upper Rhine Graben. Hence, the results of our study prove in general the applicability of outcrop analogue studies for reservoir characterization.

Among the H-type sandstones the eolian H-type sandstones from outcrops and reservoir depth exhibit the highest porosities and permeabilities (Fig. 7b, d), the highest intergranular porosity (Fig. 8b, d), the lowest illite content in the pore space (Fig. 9b, d), and the highest quartz content of 73.8 % (Tab. 2b). H-type cementation was also identified in fluvial, alluvial and playa depositional environments. The reduced porosities of alluvial H-type sandstones from reservoir depth (Fig. 7b, d) could be explained with their higher content of presumably ductile rock fragments, since rock fragment-rich sandstones lose their porosity mainly physically by mechanical compaction (Worden et al. 1997). A reason for the reduced porosities and permeabilities of fluvial H-type sandstones (Fig. 7b, d) could be their higher feldspar content (Fig. 5b). Since kaolinite and smectite alterate to permeability reducing illite at greater depth (Perry and Hower 1972, Bjørlykke 1996, Rossi et al. 2002, Worden and Morad 2000, Worden and Morad 2003) and are transformation products of feldspar in eodiagenesis (Bjørlyyke 1996), reservoir quality of sandstones is mainly controlled by the feldspar content (Rossi et al. 2002). H-type sandstones deposited under playa conditions exhibit no illite in the pore space despite high contents of feldspar (Fig. 9a, c), but their porosities are comparably low (Fig. 7a, c). This could be due to their smaller grain size (Fig 4.A2) compared to the eolian (Fig. 4.B2) and alluvial H-type sandstones. The third important influence on reservoir quality is therefore seen in the general mineral composition and the quartz content which is the highest in the Kreuznach Formation.

Mineral contents from outcrop samples suggest there are at least two different source areas for the Permocarboniferous in the Saar Nahe Basin (Fig. 5a). One source area is the Mid-German Crystalline High as part of the Saxothuringian in the southwest built of granites, granodiorites, amphibolites, mica schists and sediments (Oncken 1997) whose quartz- and feldspar-rich detritus was transported via rivers

into the basin and deposited mainly in fluvial and lacustrine environments (Fig. 5a). A second source area is the Rhenohercynian in the north mainly consisting of weakly deformed schists (Lorenz 1976, Anderle 1987). Its lithoclast-rich detritus was transported mainly alluvially and partly in eolian depositional environments into the basin. The alluvial quartz-rich sandstones are explained by the mixture with quartz-rich fluvial deposits of the Glan-Subgroup. According to Boy (2005) the alluvial fans of the Wadern Formation reached up to 14 km into the basin and mixed with other deposits. Furthermore, high feldspar contents from reservoir samples (Fig. 5b) suggest that there is another source area for the Permocarboniferous in the northern Upper Rhine Graben which could be the Moldanubian in the south built of granulites and basalts (McCann 2008).

A difference between eolian and fluvial sandstones is recognized by the evaluation of the degree of compaction since the assumed initial porosity of 40 % might be applicable for well-sorted and rounded eolian sandstones, but not for proximal alluvial to medial fluvial sandstones, where the IGV is furthermore reduced by detrital matrix. In mature sedimentary deposits of fluvial and eolian systems lower values of detrital matrix are present. However, the Permocarboniferous basin representing an internal molasse basin of the Variscan orogen is rather restricted in its size and sediment transport paths are short. Thus, the proximal to medial sediments still contain high amounts of small grain size fractions and are less mature than deposits of the Southern Permian Basin (Gaupp et al. 1993, Gaupp 1996, Schöner 2006). Hence, the sediments might in some cases be classified as “wackes” as well. Investigations by Müller (1996) of samples from the same deep wells investigated in our study showed that there is no clear correlation between grain contacts (Füchtbauer 1988) and burial depth.
In the Southern Permian Basin of Northern Germany, where rather the sedimentary end members of fluvial, alluvial and eolian systems can be expected (McCann 1998), eodiagenetic formation of haematite coatings covering grain surfaces are meant to be responsible for the preservation of high porosities at greater depth during diagenesis as well (Ehrenberg 1993, Gaupp 1996).

Measured thermal conductivities and diffusivities of the sandstones investigated are interpreted to be dominantly a function of the pore space (Buntebarth 1989). Only in rocks without pores, e.g. metamorphic, volcanic or plutonic rocks, the influence of different minerals on thermophysical parameters can be clearly identified (Clauser and Huenges 1995). Nonetheless, the database established

will allow for the identification of correlations between the modal composition or cementation types with the thermal properties of the matrix. Therefore, matrix thermal conductivities and diffusivities can be calculated based on approaches presented by Abdulagatova et al. (2009) and Fuchs et al. (2013). These would be independent of porosity and could thus be correlated with the petrography, which is a topic for future studies.

Conclusions

The present study on the Permocarboniferous of the northern Upper Rhine Graben has shown:

1. The strongest and most destructive influence on reservoir quality is related to late organic diagenetic processes. The cementation of deposits of the Glan Subgroup and the Donnersberg Formation is characterized by contamination of CO_2 bearing fluids and oil that most probably migrated from underlying Carboniferous hydrocarbon source rocks. Under these conditions, the grain covering haematite coatings were dissolved and the protection against cementation, compaction and illitisation was eliminated, resulting subsequently in the reduction of porosity and permeability during the Cenozoic subsidence of the Upper Rhine Graben.
2. The second important influence on reservoir quality is the distinct depositional environment and its influence on early diagenetic processes. Especially in eolian depositional environments the H-type cementation acts as protection against cementation, compaction and illitisation during burial and preserves the original porosity even at greater depths. These sandstones frequently occur in the Wadern, Sponheim, Kreuznach and Nierstein formations of the Nahe Subgroup and the stratigraphic units of the Sprendlinger Horst and Wetterau Basin. Eolian H-type sandstones of the Kreuznach Formation exhibit the highest porosities and permeabilities, are least compacted and show the lowest illite content.
3. The third important influence on reservoir quality is the general mineral composition and the quartz content. During burial feldspar reduces the permeability of sandstones chemically by alteration to pore filling clay minerals. On the other hand, rock fragments reduce the porosity

during mechanical compaction due to their mostly ductile behaviour. In the reservoir studied the Kreuznach Formation exhibits the highest quartz content with 73.8 %.

Only if all of these three conditions are favourably fulfilled, whose importance is contrary to their timing, good matrix reservoir qualities can be expected. Eolian H-type sandstones of the Kreuznach Formation match these criteria and are thus considered to be suitable for hydrothermal exploitation. In conclusion, the Kreuznach Formation is seen as the only horizon where the matrix permeability can contribute to the flow rate needed for future geothermal exploitation of the Permocarboniferous in the northern Upper Rhine Graben. Nonetheless, since all sandstones of the Permocarboniferous encountered in our study are strongly lithified and should therefore behave brittle when tectonically stressed, the overall formation has to be considered as a fractured aquifer and thus suitable for geothermal use. The main contribution to the required flow rates is expected from the fracture network and especially from the highly tectonized fault zones. Thus, for economic efficiency, the main targets of geothermal exploration should be faults and fractures along which sufficient fluid flow rates can be expected (Bär 2012, Aretz et al. 2013).

Acknowledgements

We gratefully thank the Bundesministerium für Umwelt, Naturschutz, Bau und Reaktorsicherheit (BMU) for funding this research project, grant no. 0325286. The Wirtschaftsverband Erdöl- und Erdgasgewinnung e.V. (WEG) is kindly acknowledged for the collaboration agreement for data exchange. ExxonMobil permitted access to its archive of drill cores and sampling and Wintershall Holding GmbH provided access to drill core data. Our thanks go to the Geological Survey of the State of Hesse (Hessisches Landesamt für Umwelt und Geologie), the Senckenberg Research Institute (Research Station Messel Pit), and the Kreuznacher Stadtwerke for giving permission to sample drill cores. We kindly acknowledge the very constructive reviews of Nicolaas Molenaar and Markus Wolfgramm, which helped to improve the manuscript significantly.

References

Abdulagatova Z, Abdulagatov IM, Emirov VN (2009) Effect of temperature and pressure on the thermal conductivity of sandstone. International Journal of Rock Mechanics and Mining Sciences 46:1055-1071

Agemar T, Schellschmidt R, Schulz R (2012) Subsurface temperature distribution in Germany. Geothermics 44:65-77

Agemar T, Brunken J, Jodocy M, Schellschmidt R, Schulz R, Stober I (2013) Untergrundtemperaturen in Baden-Württemberg. Z. Dt. Ges. Geowiss. (German J. Geosci.) 164(1):49-62

Alsop DB, Al Ghammari M, Al Abri A, Al Mahrooqi A, Al Rahwhi H, Salem H (2013) Reservoir architecture of the Gharif Formation outcrops in the Southern Huqf area, Sulanate of Oman. Geological Society, London, Special Publications 387:111-133

Anderle HJ (1987) The evolution of the South Hunsrück and Taunus Borderzone. Tectonophysics, **137**, 101-114Aretz A, Bär K, Sass I (2013) Charakterisierung des geothermischen Reservoirpotenzials des Permokarbons in Hessen und Rheinland-Pfalz – thermophysikalische und hydraulische Gesteinskennwerte. Swiss Bulletin für angewandte Geologie 18(1):33-41

Arndt D, Bär K, Fritsche J-G, Kracht M, Sass I, Hoppe A (2011) 3D structural model of the Federal State of Hesse (Germany) for geo-potential evaluation. Z. dt. Ges. Geowiss. (German J. Geosci.) 162(4):353-370

Bär K (2008) 3D-Modellierung des tiefengeothermischen Potenzials des nördlichen Oberrheingrabens und Untersuchung der geothermischen Eigenschaften des Rotliegend. unpubl. Diploma Thesis, Technische Universität Darmstadt, 141 pp.

Bär K (2012) Untersuchung der tiefengeothermischen Potenziale von Hessen. Dissertation, Technische Universität Darmstadt, 268 pp.

Bär K, Arndt D, Fritsche J-G, Götz AE, Kracht M, Hoppe A, Sass I (2011) 3D-Modellierung der tiefengeothermischen Potenziale von Hessen – Eingangsdaten und Potenzialausweisung. Z. dt. Ges. Geowiss. (German J. Geosci.) 162(4):371-388

Barcley SA, Worden RH (2000) Geochemical modeling of diagenetic reactions in subarkosic sandstone. Clay Min. 35:57-67

Barth G, Franz M, Heunisch C, Kustatscher R, Thies D, Vespermann J, Wolframm M (2014) Later Triassic (Norian-Rhaetian) brackish to fresh water habitats at a fluvial-dominated delta plain (Seinstedt, Lower Saxony, Germany). Palaeobiodiversity and Palaeoenvironments 94:495-528

Becker A, Schwarz M, Schäfer A (2012) Lithostratigraphische Korrelation des Rotliegend im östlichen Saar-Nahe-Becken. Jber. Mitt. Oberrhein. Geol. Ver. 94:105-133

Behrmann JH, Ziegler PA, Schmid SM, Heck B, Granet M [ed.] (2005) EUCOR-URGENT Upper Rhine Graben Evolution and Neotectonics. Int. J. Earth Sci. (Geol. Rdsch.) 94:505-506

Beitler B, Chan MA, Parry WT (2003) Bleaching of Jurassic Navajo Sandstone on Colorado Plateau Laramide highs: Evidence of exhumed hydrocarbon supergiants? Geology 31(12):1041-1044

Beyer D., Kunkel, C. Aehnelt, M, Pudlo, D, Voigt T, Nover G, Gaupp R (2014) Influence of depositional environment and diagenesis on petrophysical properties of clastic sediments (Buntsantstein of the Thuringian Syncline, Central Germany). Z. dt. Ges. Geowiss. 186(3):345-365

Bitzer F (2007) Ergebnisse von Durchlässigkeitsuntersuchungen an permotriassischen Gesteinen der Pfälzer Mulde. Mainzer geowiss. Mitt. 35:17-32

Bjørlykke K (1996) Clay mineral diagenesis in sedimentary basins - a key to the prediction of rock properties. Examples from the North Sea Basin. Clay minerals 33:15-34

Bjørlykke K (2010) Introduction to Sedimentology: Sediment Transport und Sedimentary Environments. In Bjørlykke (eds.): Petroleum Geoscience. 499pp.

Boy JA (2005) Geologie von Rheinland-Pfalz. 400 pp.

Buckley S, Howell JA, Enge H, Tobias K (2008) Terrestrial laser scanning in geology: data acquisition, processing and accuracy consideration. Journal of the Geological Society 165:625-638

Buntebarth G (1989) Geothermie – Eine Einführung in die allgemeine und angewandte Wärmelehre des Erdkörpers. 156 pp.

Chan MA, Parry WT, Bowman JR (2000) Diagenetic Hematite and Manganese Oxides and Fault-Related Fluid Flow in Jurassic Sandstones, Southeastern Utah. AAPG Bull. 84(9):1281-1310

Clauser C, Villinger H (1990) Analysis of conductive and convective heat transfer in a sedimentary basin, demonstrated for the Rheingraben. Geophys. J. Int. 100:393-414

Clauser C, Huenges E (1995) Thermal conductivity of Rocks and Minerals. Rock Physics and Phase Relations, A Handbook of Physical Constants. AGU Reference Shelf 3:105-126

Clemmensen LB (1987) Complex star dunes and associated aeolian bedforms, Hopeman Sandstone (Permo-Triassic), Moray Fifth Basin, Scotland. Geological Society, London, Special Publications 35:213-231

Cookenboo HO, Bustin RM (1999) Pore water evolution in sandstones of the Groundhog Coalfield, northern Bower Basin, British Columbia. Sed. Geol. 123:129-146

Deutsche Gesellschaft für Geotechnik e.V. / Deutsche Gesellschaft für Geowissenschaften e.V. (eds.): Empfehlung Oberflächennahe Geothermie – Planung, Bau, Betrieb und Überwachung – EA Geothermie. 290 pp.

Dreyer T (1990) Sand body dimensions and infill sequences of stable, humid-climate delta plain channels. North Sea Oil and Gas Reservoirs – II:337-351

Ehrenberg SN (1993) Preservation of anomalously high porosity in deeply buried sandstones by grain coating chlorite: Examples from the Norwegian Continental Shelf. AAPG Bulletin 77:1260-1286

Emery D, Smalley PC, Oxtoby NH (1993) Synchronous oil migration and cementation in sandstone reservoir demonstrated by quantitative description of diagenesis. Philosophical Transactions of the Royal Society of London A 344:125-135

Enge HD, Buckley SJ, Rotevatn A, Howell JA (2007) From outcrop to reservoir simulation model: workflow and procedures. Geosphere 3:469-490

Eschard R, Deschamps R, Doligez B, Lerat O (2013) Connectivity estimation between turbiditic channels and overbank deposits from the modelling of an outcrop analogue (Pab Formation, Maastrichitan, Pakistan). Geological Society, London, Special Publications 387(1):203-231

Evans JP, Forster CB, Goddard JV (1997) Permeability of fault-related rocks and implications for hydraulic structure of fault zones. J. Struct. Geol 19:1393–1404

Fielding CR, Crane RC (1987) An application of statistical modeling to the prediction of hydrocarbon recovery factors in fluviatil reservoir sequences. Recent Developments in Fluviatil Sedimentology 39:321-327

Filomena CM, Hornung J, Stollhofen H (2014) Assessing accuracy of gas-driven permeability measurements: a comparative study of diverse Hassler-cell and probe permeameter devices. Solid Earth 5(1):1-11

Foxford KA, Garden IR, Guscott SC, Burley SD, Lewis JJM, Walsh JJ, Watterson J (1996) The Field Geology of the Moab Fault. In: Huffman AC, Lund WR, Godwin LH (eds.): Geology and Resources of the Paradox Basin, Utah Geol. Assoc. Guidebook 25:256-283

Fuchs S, Schütz F, Förster HJ, Förster A (2013) Evaluation of mathematical models for predicting thermal conductivity of sedimentary rocks. Correction charts and new conversion equations. Geothermics 47:40–52.

Füchtbauer H. (1988) Sedimente und Sedimentgesteine. 1141 pp.

Garden IR, Guscott SC, Burley SD, Foxford KA, Walsh JJ, Marshall J (2001) An exhumed palaeo-hydrocarbon migration fairway in a faulted carrier system, Entrada Sandstone of SE Utah, USA. Geofluids 1:195-213

Gaupp R, Matter A, Platt J, Ramseyer K, Walzebuck J (1993) Diagenesis and Fluid Evolution of Deeply Buried Permian (Rotliegend) Gas Reservoirs, Northwest Germany. AAPG Bulletin 77(7):1111-1128

Gaupp R (1996) Diagenesis types and their application in diagenesis mapping. Zbl. Geol. Paläont., Teil 1(11/12):1183-1199

GeORG-Projektteam (2013): Geopotenziale des tieferen Untergrundes im Oberrheingraben, Fachlich-Technischer Abschlussbericht des Interreg-Projekts GeORG, Teil 2: Geologische Ergebnisse und Nutzungsmöglichkeiten. 346 pp.

Gibling MR (2006) Width and thickness of fluvial channel bodies and valley fills in the geological record: a literature compilation and classification. Journal of Sedimentary Research 76:731-770

Grobe R, Bauer JF, Bechstädt T, Fensterer M, Kissner T, Meier S, Miernik G, Philipp SL, Reinecker J, Soyk D, Stollhofen H, Wenke A (2013) Aufschlussanalogstudien und ihre Anwendbarkeit in der geothermischen Exploration – AuGE. Proceedings „Der Geothermiekongress 2013“, Essen, 7 pp.

Grötsch J, Gaupp R (2011) Foreword by the editors. In Grötsch J & Gaupp R. (eds.): The Permian Rotliegend of the Netherlands. SEPM Special Publications 98:3-6

Hänel R, Staroste E (1988 and 2002) Atlas of Geothermal Resources in the European Community, Austria and Switzerland. Publ. No. EUR 11026 und 17811 of the European Commission Office of Official Publications of the European Communities, Luxemburg

Hasner K (2004) Untersuchungen an Hämatit-Tonmineralkrusten in Rotliegendsandsteinen des Norddeutschen Beckens. Diploma Thesis, Friedrich-Schiller-Universität Jena, 141 pp.

Hartmann A, Rath V, Clauser C (2005) Thermal conductivity from core and well log data. International Journal of Rock Mechanics & Mining Sciences 42:1042-1055

Henk A (1992) Mächtigkeit und Alter der erodierten Sedimente im Saar-Nahe-Becken (SW-Deutschland). Geologische Rundschau 81(2):323-331

Henk A (1993a) Subsidenz und Tektonik des Saar-Nahe-Beckens (SW-Deutschland). Geol. Rundsch. 82:3-19

Henk A (1993b) Late orogenic basin evolution in the Variscan Internides: the Saar-Nahe Basin, southwest Germany. Tectonophysics 223:273-290

Hertle M (2003) Numerische Simulation der geologischen Entwicklungsgeschichte des permokarbonen Saar-Nahe-Beckens. Dissertation, RWTH Aachen, 154 pp.

Hodgetts D (2013) Laser scanning and digital outcrop geology in the petroleum industry: a review. Marine and Petroleum Geology 46:335-354

Homuth S, Götz AE, Sass I (2014) Lithofacies and depth dependency of thermo- and petrophysical rock parameters of the Upper Jurassic geothermal carbonate reservoirs of the Molasse Basin. Z. dt. Ges. Geowiss. (German J. Geosci.) 165:469-486

Houseknecht DW (1987) Assessing the relative importance of compaction processes and cementation to reduction of porosity in sandstones. AAPG Bull. 71(6):633-642

Houseknecht DW (1988) Intergranular pressure solution in four quartzose sandstones. Journal of Sedimentary Petrology 58:228-246

Hurter S, Schellschmidt R (2003) Atlas of geothermal resources in Europe. Geothermics 32(4–6):779–787

Howell JA, Allard WM, Good TR (2014) The application of outcrop analogues in geological modeling: a review, present status and future outlook. Geological Society, London, Special Publications 387:1-25

Illies, JH (1972) The Rhine graben rift system - plate tectonics and transform faulting. Geophysical surveys 1:27-60

Jahn F, Graham M, Cook M (2008) Hydrocarbon Exploration & Production. 432 pp.

Klinkenberg LJ (1941) The permeability of porous media to liquids and gases. Drilling Production Practice, API:200-213

Koegh KJ, Leary S, Martinius AW, Scott ASJ, Riordan, S, Voste I, Gowland S, Taylor AM, Howell J (2014) Data capture for multiscaling modeling of the Lourinha Formation, Lusitanian Basin, Portugal: an outcrop analogue for the Stratfjord Group and future directions. Geological Society, London, Special Publications 387:27-56

Kowalczyk G (2001) Permokarbon des Sprendlinger Horstes und der westlichen Wetterau (Exkursion I am 20. April 2001). Jber. Mitt. Oberrhein. geol. Ver. 83:211-236

Langmuir, D. (1997): Aqueous environmental geochemistry. Prentice Hall, New Jersey, 600 Seiten

Lippmann E, Rauen A (2005) TCS manual / Handbuch zum Thermal Conductivity Scanner

Littke R, Brauckmann FJ, Radke M, Schaefer RG (1996) Solid bitumen in Rotliegend gas reservoirs in Northern Germany: implications for their thermal and filling history. Zbl. Geol. Paläont. 1(11/12):1275-1291

Lockner DA, Naka H, Tanaka H, Ito H, Ikeda R (2000) Permeability and strength of core samples from the Nojima fault of the 1995 Kobe earthquake. In: GSJ Internal Report No. EQ/00/1, Proceedings of the Internal Workshop on Nojima Fault Core and Borehole Date Analysis 147-157

Lorenz V (1976) Formation of Hercynian subplates, possible causes and consequences. Nature, 262, 374-377

Lützner H, Kowalczyk G (2012) Stratigraphie von Deutschland X, Rotliegend, Teil 1: Inner-variscische Becken. Schriftenreihe der Deutschen Gesellschaft für Geowissenschaften 61:882 pp.

McCann T (1998) Sandstone and provenance of the Rotliegend of the NE German Basin. Sedimentary Geology 116:177-198

McCann T (2008) The Geology of Central Europe: Precambrian and Palaeozoic. The Geological Society, ISBN 978-1862392458, 748 pp.

Marell D (1989) Das Rotliegende zwischen Odenwald und Taunus. Geol. Abh. Hessen 89:128 pp.

Metcalfe R, Rochelle CA, Savage D. und Higgo JW (1994) Fluid-rock interactions during continental red bed diagenesis: implications for theoretical models of mineralization in sedimentary basins. In: Parnell, J.: Geofluids: Origin, Migration and Evolution of Fluids in Sedimentary Basins. Geological Society Special Publications, **78**, 301-324

Miall AD (1996) The Geology of Fluvial Deposits. 582 pp.

Molenaar N (1998) A review of effects of diagenesis on petrophysical properties and reservoir quality and the controls on diagenesis. Nordic Petroleum Technology Series 5:155-170

Morad S (1998): Carbonate cementation in sandstones: Distribution Patterns and Geochemical Evolution. IAS Spec. Pub. 26:1-26

Mountney N, Howell JA, Flint SS, Jerram V (1999) Relating eolian bounding-surface geometries to the bed forms that generated them: Etjo Formation, Cretaceous, Namibia. Geology 27:159-162

Müller H (1996) Das Permokarbon im nördlichen Oberrheingraben – Paläogeographische und strukturelle Entwicklung des permokarbonen Saar-Nahe-Beckens im nördlichen Oberrheingraben. Geol. Abh. Hessen 99:86 pp.

Oncken O (1997) Transformation of a magmatic arc and an orogenic root during oblique collision and its consequences for the evolution of the European Variscides (Mid-German Crystalline Rise). Geol. Rdsch., 86, 2-20

Pape HG, Clauser C, Iffland J (1999): Permeability prediction based on fractal pore space geometry. Geophysics 64(5):1447-1460

Parry WT, Chan MA, Beitler B (2004) Chemical bleaching indicates episodes of fluid flow in deformation bands in sandstone. AAPG Bull. 88(2):175-191

Paxton ST, Szabo JO, Ajdukiewicz JM, Klimentidis RE (2002) Construction of an intergranular volume compaction curve for evaluating and predicting compaction and porosity loss in rigid-grain sandstone reservoirs. AAPG Bulletin 86:2047-2067

Perry EA, Hower J (1972) Late-stage dehydration in deeply buried pelitic sediments. AAPG Bulletin 56:2013-2012

Pettijohn FJ (1975) Sedimentary rocks. 628 pp.

Plein E, Adrichem Boogaert A, van Bachman GH, Benek R, Döring H, Ellenberg J, Gaiztsch B, Gast RU, Geluk M, Helmuth HJ, Hoffmann N, Hoth K, Huebscher HD, Kleditzsch O, Korich D, Kramer W, Lützner H, Marx J, Menning M, Pasternak M, Schneider J, Schretzmayr S, Süssmuth S (1995) Norddeutsches Rotliegendbecken. Rotliegend-Monographie Teil 22. Courier Forsch.-Inst. Senckenberg, 183, 1-193, Frankfurt am Main

Popov YA, Pribnow DFC, Sass JH, Williams, CF, Burkhardt H (1999) Complex detailed Investigations of the thermal properties of Rocks on the basis of a moving point Source. Earth Physics 21(1)

Popov YA, Tertychnyi V, Romushkevich R, Korobkov D, Pohl J (2003) Interrelations Between Thermal Conductivity and Other Physical Properties of Rocks: Experimental Data. Pure Applied Geophysics 160:1137-1161

Pranter MJ, Hewlett AC, Cole RD, Wang H, Gilman J (2013) Fluvial architecture and connectivity of the Williams Form Formation: use of outcrop analogues for stratigraphic characterization and reservoir modeling. Geologic Society, London, Special Publications 387:57-83

Pribnow D, Schellschmidt R (2000) Thermal tracking of upper crustal fluid flow in the Rhine Graben. Geophysical Research Letters 27(13):1957-1960

Rawling GC, Goodwin LB, Wilson JL (2001) Internal architecture, permeability structure, and hydrologic significance of contrasting fault-zone types. Geology 29(1):43-46

Reading HG (1996) Sedimentary environments - processes, facies and stratigraphiy. 688 pp.

Rohrer L (2010) Seismische Interpretation und Aufschluss-Analogstudie des Rotliegend im nördlichen Oberrheingraben und im Saar-Nahe-Becken. Diploma thesis, Universität Heidelberg, 86 pp.

Rossi C, Kälin O, Aaribas J, Tortusa A (2002) Diagenesis, provenance and reservoir quality of Triassic TAGI sandstones from Ourhood field, Berkine (Ghadames) Basin, Algeria. Marine and Petroleum Geology 19:117-142

Sass I, Hoppe A (2011) Forschungs- und Entwicklungsprojekt „3D-Modell der geothermischen Tiefenpotenziale von Hessen" Abschlussbericht (http://www.energieland.hessen.de/mm/3-D-Modell-Hessen-Endbericht_(PDF,_7.300_KB).pdf) [December 2013]

Sass I, Götz AE (2012) Geothermal reservoir characterization: a thermofacies concept. Terra Nova 24:142-147

Schäfer A (1980) Sedimenttransport im Permokarbon des Saar-Nahe-Beckens (Oberkarbon und Unterrotliegendes) – Konsequenz für die Entwicklung des Ablagerungsraumes. Z. Dt. Geol. Ges. 131:815-841

Schäfer A (1986) Die Sedimente des Oberkarbons und Unterrotliegenden im Saar-Nahe-Becken. Mainzer Geowissenschaftliche Mitteilungen 15:239-365

Schäfer A (1989) Variscan molasse in the Saar-Nahe Basin (W-Germany), Upper Carboniferous and Lower Permian. Geol. Rdsch. 78:499-524

Schäfer A (2005) Sedimentologisch-numerisch begründeter Stratigraphischer Standard für das Permo-Karbon des Saar-Nahe-Beckens. Cour. Forsch.-Inst. Senckenberg 254:369-394

Schäfer A (2011) Tectonics and sedimentation in the continental strike-slip Saar-Nahe Basin (Carboniferous-Permian, West Germany). Z. dt. Ges. Geowiss. 162(2):127-155

Scheffer F. und Schachtschabel P. (1992) Lehrbuch der Bodenkunde, 13th ed., Ferdinand Enke-Verlag, ISBN 978-3-8274-1444-1, 442 pp., Stuttgart

Schmidt RB, Seithel R, Bucher K, Stober I (2015) Fluid-rock interaction in deep fault systems and the influence on permeability in typical rocks of the Upper Rhine Graben, southwest Germany. Proceedings World Geothermal Congress 2015, Melbourne, Australia. 5 pp.

Schöner R (2006) Comparison of Rotliegend sandstone diagenesis from the northern and southern margin of the North German Basin, and implications for the importance of organic maturation and migration. PhD Thesis, Friedrich-Schiller-University Jena, 160 pp.

Schulz R, Knopf S, Suchi E, Dittmann J (2013) Geothermieatlas zur Darstellung möglicher Nutzungskonkurrenzen zwischen CCS und Tiefer Geothermie. Leibniz-Institut für Angewandte Geophysik und Bundesanstalt für Geowissenschaften und Rohstoffe. 108 pp.

Schwarz M, Becker A, Schäfer A (2011) Seismische Leithorizonte im nordöstlichen Saar-Nahe-Becken. Erdöl Erdgas Kohle 127:28-34

Stapf KRG (1982) Schwemmfächer- und Playa-Sedimente im Ober-Rotliegenden des Saar-Nahe-Beckens (Permokarbon, SW-Deutschland). Ein Überblick über Faziesanalyse und Faziesmodell. Mitteilungen über Pollichia 70:7-54

Stober I, Bucher K (2007) Hydraulic properties of the crystalline basement. Hydrogeology Journal 15:213–224

Stober I, Jodocy M (2009) Eigenschaften geothermischer Nutzhorizonte im baden-württembergischen und französischen Teil des Oberrheingrabens. Grundwasser 14:127–137

Stollhofen H (1994) Synvulkanische Sedimentaton in einem fluviatilen Ablagerungsraum: Das basale „Oberrotliegend“ im permokarbonen Saar-Nahe-Becken. Z. dt. geol. Ges. 145:343-378

Stollhofen H (1998) Facies architecture variations and seismogenic structures in the Carboniferous-Permian Saar-Nahe Basin (SW Germany): evidence for extension-related transfer fault activity. Sedimentary Geology 119:47-83

Surdam RC, Boese SW, Crossey LJ (1984) The chemistry of secondary porosity. In: McDonald, DA, Surdam, RC (eds.), Clastic Diagenesis. AAPG Memoir 37:127-149

Stumm W (1992) Chemistry of the solid-water interface: Processes at the mineral-water and particle-water interface in natural systems. Wiley, ISBN 0-471-57672-7, 428 pp., New York

Teichmüller M, Teichmüller R (1979) Zur geothermischen Geschichte des Oberrheingrabens. Zusammenfassung und Auswertung eines Symposiums. Fortschr. Geol. von Rheinld u. Westf. 2:109-120

Turner P (1980) Continental red beds, Developments in sedimentology – 29th ed., Elsevier, ISBN 978-0-444-41908-8, 562 pp.

Velde B (1995) Origin and mineralogy of clays. 334 pp.

van Houten FB (1973) Origin of red beds. A review – 1961 – 1972. Ann. Rev. Earth Planet. Sci. 1:39-61

Walter R, Dorn P (2007) Geologie von Mitteleuropa. 511 pp.

Weibel R (1999) Pseudomorphous transformation of goethite needles into hematite in sediments of the Traissic Skagerrak Formation, Denmark. Clay Minerals 34: 657-660

Wenke A, Gall W, Gutekunst S, Kreuter H, Rohrer L, Zühlke R. (2009) Tiefe Geothermie im Raum Groß-Gerau – Erkenntnisse einer ersten Reconnaissance Studie. Proceedings – Der Geothermiekongress 2009, Technikforum 8 – Exploration III, Bochum, 17.-19.11.2009

Wenke A, Spath F, Aichinger J, Bißmann S, Grobe R, Kreuter H, Lorson C, Rohrer L, Rothert E, Schrage C, Zöllner E, Zühlke R (2011) Geologische Erkenntnisse und neuere Entwicklungen im Erlaubnisfeld Groß-Gerau. Präsentation 6. Hessisches Tiefengeothermieforum

Wolfgramm M (2005) Fluidentwicklung und Diagenese im Nordostdeutschen Becken – Petrographie, Mikrothermometrie und Geochemie stabiler Isotope. PhD Thesis, Martin-Luther-Universität Halle-Wittenberg. 170 pp.

Worden RH, Mayall MJ, Evans IJ (1997) Predicting reservoir quality during exploration: lithic grains, porosity and permeability in Tertiary clastics of the South Chine Sea basin. Geological Society, London, Special Publications 126:107-115

Worden RH, Barcley SA (2000) Internally-sourced quartz cement due to externally-derived CO_2 in sub-arkosic sandstones, North Sea. Journal of Geochemical Exploration 69-70:645-649

Worden RH, Morad S (2000) Quartz cementation in oil field sandstones: a review of the key controversies. Spec. Publs int. Ass. Sediment 29:1-20

Worden RH, Morad S (2003) Clay Mineral Cements in Sandstones. IAS Spec. Pub. 34:1-520.

Ziegler PA (1990) Geological Atlas of Western and Central Europe. Shell Internationale Petroleum Maatschappij, B.V., ISBN 9789066441255, 239 pp.

Table 1. Petrophysical parameters of the stratigraphic units of the Permocarboniferous; a) outcrop samples and b) samples taken from reservoir depth. Θ = porosity. Κ = permeability. λ = thermal conductivity. κ = thermal diffusivity. Ble = Bleichenbach beds of the Wetterau Basin. Ni = Nierstein Formation. Kr = Kreuznach Formation. Sp = Sponheim Formation. Wa = Wadern Formation. La = Langen beds of the Sprendlinger Horst. Do = Donnersberg Formation. Th = Thallichtenberg Formation. Ob = Oberkirchen Formation. Di = Disibodenberg Formation. Me = Meisenheim Formation. Od = Odernheim Formation. Je = Jeckenbach Formation. Lau = Lauterecken Formation. Qb = Quirnbach Formation. Wah = Wahnwegen Formation. Alt = Altenglan Formation. Rem = Remigiusberg Formation.. min = minimum. mn = mean value. std = standard deviation. max = maximum. n = number of samples.

a	**Θ [%]**					**Κ [m²]**					**λ [w/(m·K)]**					**κ [E-6 m²/s]**				
	min	mn	std	max	n	min	mn	std	max	n	min	mn	std	max	n	min	mn	std	max	n
Ble	2.1	14.3	5.1	19.8	42	4.1E-18	1.2E-15	4.1E-14	1.7E-13	47	1.34	1.99	0.53	3.16	58	0.62	1.12	0.20	1.47	59
Sch	11.9	16.1	5.9	23.4	9	8.4E-16	2.6E-15	3.0E-14	8.3E-14	9	1.42	1.77	0.58	2.22	9	0.83	0.94	0.31	1.19	9
La	6.0	13.6	3.4	20.0	94	8.8E-18	1.7E-16	2.5E-15	1.1E-14	31	1.84	2.36	0.36	3.26	96	0.80	1.24	0.28	1.97	96
Mo	3.4	9.0	3.1	11.8	11	5.9E-18	4.7E-15	2.0E-14	6.0E-14	11	1.82	2.16	0.94	4.27	11	0.65	0.98	0.39	1.77	11
Ni	-	-	-	-	0	-	-	-	-	0	-	-	-	-	0	-	-	-	-	0
Kr	7.3	16.3	3.5	23.8	106	5.5E-18	2.9E-15	2.8E-14	1.3E-13	73	1.48	2.04	0.25	2.74	132	0.60	1.17	0.14	1.54	134
Sp	6.0	10.0	3.6	18.1	13	7.0E-18	2.6E-17	2.7E-15	6.5E-15	8	1.33	2.15	0.39	2.50	13	0.70	1.24	0.25	1.45	13
Wa	1.0	15.3	6.8	22.1	50	1.0E-18	2.3E-15	2.1E-14	5.8E-14	50	1.40	2.59	0.53	5.03	50	0.91	1.76	0.36	2.77	50
Do	4.1	13.4	3.7	21.2	118	1.0E-18	4.0E-16	7.2E-15	5.2E-14	53	1.40	2.43	0.37	3.26	118	0.79	1.35	0.32	2.42	118
Th	12.8	19.1	2.5	22.3	77	1.7E-17	1.4E-15	6.2E-14	5.2E-13	75	1.68	2.19	0.32	3.06	75	1.06	1.41	0.21	1.87	79
Ob	6.9	16.1	3.5	20.9	47	5.2E-17	2.9E-15	8.0E-15	2.5E-14	47	1.87	2.47	0.38	3.06	46	1.12	1.60	0.24	2.19	47
Di	13.4	15.4	1.5	19.8	25	2.2E-16	5.3E-16	5.9E-16	3.2E-15	22	1.93	2.26	0.22	259	25	1.16	1.43	0.16	1.72	24
Me	-	-	-	-	0	-	-	-	-	0	-	-	-	-	0	-	-	-	-	0
Od	11.7	15.7	3.4	19.5	10	1.9E-17	1.0E-15	4.0E-16	2.4E-16	11	1.59	1.92	0.24	2.25	9	0.90	1.13	0.15	1.31	9
Je	2.7	14.2	5.5	23.1	98	1.0E-18	3.5E-16	6.7E-15	5.3E-14	107	1.73	2.44	0.29	3.12	111	1.03	1.50	0.27	2.84	98
Lau	1.5	13.4	4.3	23.5	69	1.0E-18	3.6E-16	3.6E-15	1.4E-14	71	1.68	2.31	0.38	3.59	67	0.98	1.38	0.33	2.48	32
Qb	3.0	10.0	6.0	18.2	27	4.0E-18	1.3E-16	1.9E-15	5.4E-15	18	1.95	2.78	0.43	3.29	28	1.21	1.62	0.23	2.35	32
Wa	13.6	17.8	2.7	20.4	22	5.1E-16	7.7E-16	7.8E-15	2.3E-14	10	1.66	2.19	0.43	2.83	22	0.88	1.27	0.25	1.91	18
Alt	0.1	4.2	3.7	17.0	55	1.0E-18	1.0E-18	2.0E-16	1.1E-15	53	1.95	2.56	0.22	3.04	52	0.80	1.30	0.21	2.11	52
Re	12.1	16.4	2.3	18.2	7	5.3E-16	3.8E-15	2.0E-15	5.4E-15	6	1.99	2.15	0.11	2.34	7	1.30	1.38	0.09	1.57	7
b	**Θ [%]**					**Κ [m²]**					**λ [w/(m·K)]**					**κ [E-6 m²/s]**				
	min	mn	std	max	n	min	mn	std	max	n	min	mn	std	max	n	min	mn	std	max	n
Ni	6.7	7.2	0.7	7.7	2	3.8E-18	9.6E-18	8.2E-18	1.5E-17	2	2.54	2.63	0.13	2.78	3	1.57	1.65	0.07	1.69	3
Kr	5.6	14.0	4.3	17.5	11	9.6E-17	1.6E-15	2.2E-15	7.7E-15	11	2.16	2.45	0.36	3.28	14	1.32	1.59	0.17	1.90	13
Sp	2.3	7.6	5.3	12.7	4	3.7E-18	2.6E-17	4.0E-17	9.3E-17	4	2.05	2.17	0.15	2.35	5	1.15	1.33	0.22	1.70	5
Wa	7.1	8.5	1.2	9.3	3	3.1E-15	8.2E-15	4.9E-15	1.3E-14	3	1.68	2.04	0.31	2.23	3	0.92	1.29	0.32	1.49	3
Do	0.8	6.3	3.2	10.9	11	1.0E-18	1.6E-17	3.1E-15	1.0E-14	11	2.13	2.41	0.31	2.98	11	1.05	1.36	0.27	1.99	11
Th	-	-	-	-	0	-	-	-	-	0	-	-	-	-	0	-	-	-	-	0
Ob	-	-	-	-	0	-	-	-	-	0	-	-	-	-	0	-	-	-	-	0
Di	1.8	1.8		1.8	1	1.4E-18	1.4E-18		1.4E-18	1	2.88	2.88		2.88	1	1.44	1.44		1.44	1
Me	0.1	2.3	2.2	5.1	7	1.0E-18	1.0E-18	5.4E-16	1.4E-15	7	2.44	2.80	0.42	3.55	9	1.07	1.40	0.34	2.14	9
Od	0.2	2.0	1.2	3.3	7	1.0E-18	1.1E-17	1.2E-17	2.5E-17	7	2.27	2.52	0.26	2.89	7	0.98	1.20	0.20	1.48	7
Je	3.0	3.6	0.9	4.2	2	3.7E-18	3.7E-18		3.7E-18	1	3.1	3.1		3.1	1	1.6	1.6		1.6	1
Lau	0.4	2.8	3.1	6.2	3	1.0E-18	6.1E-18	2.4E-16	4.1E-16	3	2.86	2.92	0.05	2.96	3	1.30	1.58	0.25	1.79	3

Table 2. Petrographic composition of sandstones listed according to the stratigraphic units; a) outcrop samples and b) samples taken from reservoir depth. Gr = grain content. Qt = quartz. Pl = plagioclase. Ka = Kalifeldspar. Lt = lithic rock fragments. Mi = mica. Ca = calcite. Ma = matrix. GM = grain plus matrix content. Ce = cement content. Cc = calcitic cement. Dc = dolomitic cement. Hc = haematite cement. Ic = illitic cement. Bc = bitumina cement. Qc = quartzitic cement. Kc = kaolinitic cement. θ = Intergranular porosity. n = number of samples. For details on the abbreviations of stratigraphic units see Table 1.

a	**Kg**	**Qz**	**Pl**	**Ka**	**Lt**	**Gl**	**Kt**	**Ma**	**KM**	**Zg**	**Klz**	**Dz**	**Hz**	**Iz**	**Bz**	**Qz**	**Kz**	**θ**	**n**
Ble	**46.2**	22.6	9.0	8.4	5.3	0.6	0.3	19.6	**65.8**	**29.4**	6.9	1.4	21.0	0.1	0.0	0.0	0.0	**4.7**	3
Sch	**72.1**	51.3	2.5	9.9	8.2	0.1	0.2	2.2	**74.3**	**15.6**	6.9	0.1	5.6	2.5	0.2	0.0	0.3	**10.1**	4
La	**60.8**	43.1	4.8	1.2	5.9	1.9	3.9	**2.5**	**63.3**	**23.0**	8.8	0	10.7	3.6	0.0	0.0	0.0	**13.7**	4
Mor	**72.2**	31.1	12.7	5.1	21.1	1.5	0.7	4.8	**77.0**	**20.6**	9.7	1.4	7.2	2.0	0.1	0.0	0.2	**2.3**	4
Ni	**-**	-	-	-	-	-	-	**-**	**-**	**-**	-	-	-	-	-	-	-	**-**	0
Kr	**60.7**	36.1	5.2	4.1	15.1	0.2	0.1	**8.0**	**68.7**	**18.1**	3.9	0	13.2	0.8	0.0	0.2	0.0	**13.2**	15
Sp	**70.4**	12.4	1.2	2.9	53.7	0	0.3	**4.2**	**74.6**	**19.1**	3.8	0	15.2	0	0.0	0.1	0.0	**6.3**	2
Wa	**71.8**	37.2	1.4	3.7	26.8	0.6	2.2	**5.2**	**77.0**	**13.3**	1.2	0.1	3.4	3.5	0.0	0.2	5.0	**9.7**	8
Do	**64.6**	43.3	3.7	8.7	7.5	1.2	0.1	**11.7**	**76.3**	**14.1**	0.2	4.1	0.1	5.5	3.5	0.8	0.0	**9.7**	4
Th	**61.0**	38.0	2.7	7.3	9.0	3.5	0.4	**8.7**	**69.7**	**20.4**	3.6	0	3.5	4.6	6.9	1.1	0.8	**9.9**	9
Ob	**70.9**	43.9	3.7	15.8	6.1	1.2	0	**3.7**	**74.6**	**16.1**	4.0	0.4	0.4	2.7	5.0	0.5	3.1	**9.3**	6
Di	**68.2**	40.7	6.3	7.7	7.7	5.8	0	**8.3**	**76.5**	**13.6**	0.2	0	1.1	6.4	3.7	0.4	1.8	**9.8**	4
Me	**-**	-	-	-	-	-	-	**-**	**-**	**-**	-	-	-	-	-	-	-	**-**	0
Od	**61.2**	26.5	6.2	9.3	11.4	7.2	0.4	**12.3**	**73.5**	**20.9**	13.	0	0.6	3.0	3.8	0.0	0.0	**5.6**	1
Je	**64.7**	34.3	9.9	6.7	9.4	4.1	0.2	**11.4**	**76.1**	**19.1**	2.8	0	3.3	8.1	4.0	0.8	0.0	**4.9**	9
Lau	**60.4**	31.7	7.3	6.1	10.8	4.4	0.1	**15.2**	**75.6**	**18.0**	4.2	0	2.3	6.8	4.1	0.7	0.0	**6.4**	8
Qb	**71.2**	37.1	12.2	5.9	8.9	5.5	1.7	**6.0**	**77.2**	**19.0**	10.	0	0.1	2.9	5.5	0.0	0.0	**5.5**	2
Wah	**72.2**	49.2	5.4	5.4	10.5	1.7	0	**2.0**	**74.2**	**9.5**	0.7	0	0	0	8.8	0.0	0.0	**16.3**	1
Alt	**54.0**	27.5	5.0	5.4	7.6	8.4	0	**22.8**	**76.8**	**21.2**	2.9	0	0.2	15.	2.5	0.1	0.0	**1.6**	3
Rem	**68.6**	41.4	4.9	5.6	13.9	2.8	0	**1.6**	**70.2**	**11.2**	0	0	0.5	3.3	7.4	0.0	0.0	**18.6**	1
b	**Gr**	**Qt**	**Pl**	**Al**	**Lt**	**Mi**	**Ca**	**Ma**	**GM**	**Ce**	**Cc**	**Dc**	**Hc**	**Ic**	**Bc**	**Qc**	**Kc**	**θ**	**n**
Ni	**-**	-	-	-	-	-	-	**-**	**-**	**-**	-	-	-	-	-	-	-	**-**	0
Kr	**66.9**	49.4	4.4	2.1	10.6	0.3	0.0	**2.4**	**69.3**	**10.7**	0	0	4.0	3.9	0	2.8	0	**20.0**	5
Sp	**36.8**	24.1	6.0	2.5	2.2	0.8	1.3	**24.9**	**61.7**	**35.2**	6.9	0	11.9	15.	0	0.7	0	**3.2**	2
Wa	**73.7**	27.2	11.7	6.2	25.7	0.7	2.1	**0.6**	**74.3**	**11.4**	1.2	0	8.7	1.4	0	0.1	0	**14.3**	3
Do	**76.3**	25.4	17.0	6.6	21.3	2.7	3.4	**2.0**	**78.3**	**20.1**	5.4	2.2	2.6	5.5	1.9	2.4	0	**1.6**	10
Th	**-**	-	-	-	-	-	-	**-**	**-**	**-**	-	-	-	-	-	-	-	**-**	0
Ob	**-**	-	-	-	-	-	-	**-**	**-**	**-**	-	-	-	-	-	-	-	**-**	0
Di	**79.5**	26.5	21.9	4.1	14.6	2.7	9.7	**1.1**	**80.6**	**18.9**	2.4	1.4	0.8	13.	0.0	0.5	0	**0.5**	1
Me	**63.6**	35.0	8.0	5.4	7.3	1.2	6.7	**6.1**	**69.7**	**29.8**	0	3.9	16.8	8.6	0.3	0.3	0	**0.4**	5
Od	**73.9**	15.7	23.8	3.0	9.2	21.	1.0	**3.8**	**77.7**	**22.2**	7.6	0.3	3.4	5.1	2.2	3.7	0	**0.1**	5
Je	**74.4**	22.3	32.9	5.4	7.5	1.8	4.2	**0.7**	**75.1**	**24.7**	13.	1.6	7.8	0.5	0.9	0.2	0	**0.2**	1
Lau	**81.2**	32.9	16.1	3.2	17.1	3.6	8.2	**1.5**	**82.7**	**17.4**	1.9	2.4	0.4	10.	0.0	2.5	0	**0**	3

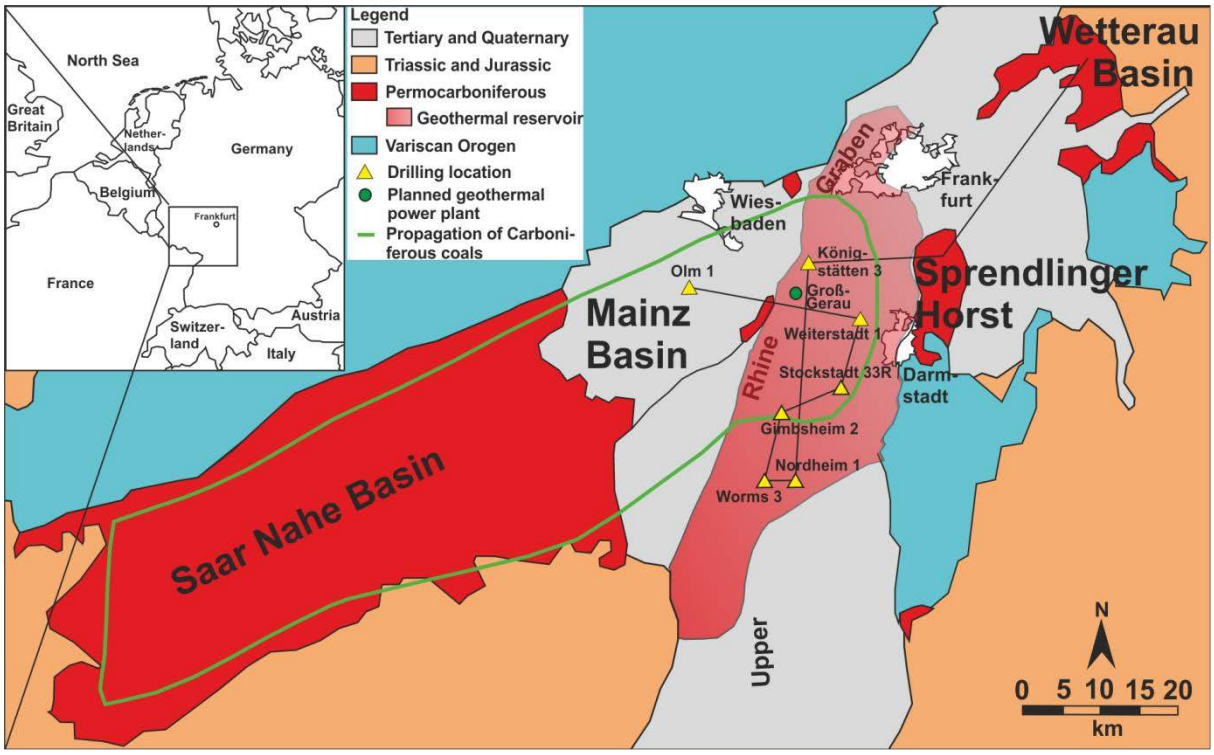

Fig. 1. Simplified geological overview map of the northern Upper Rhine Graben in SW Germany. In this area the top of the Permocarboniferous reservoir is located in a depth of 600 to 2,990 m (red shaded area). The modelled reservoir temperatures exceed 150 °C (Arndt et al. 2011) making it suitable for hydrothermal power production. The adjacent areas (Saar Nahe Basin, Sprendlinger Horst and Wetterau Basin) where the Permocarboniferous is exposed in outcrops are the targets of the outcrop analogue studies. Occurrence of Carboniferous coals after Müller (1996). Profiles along the indicated transect are shown in figure 2.

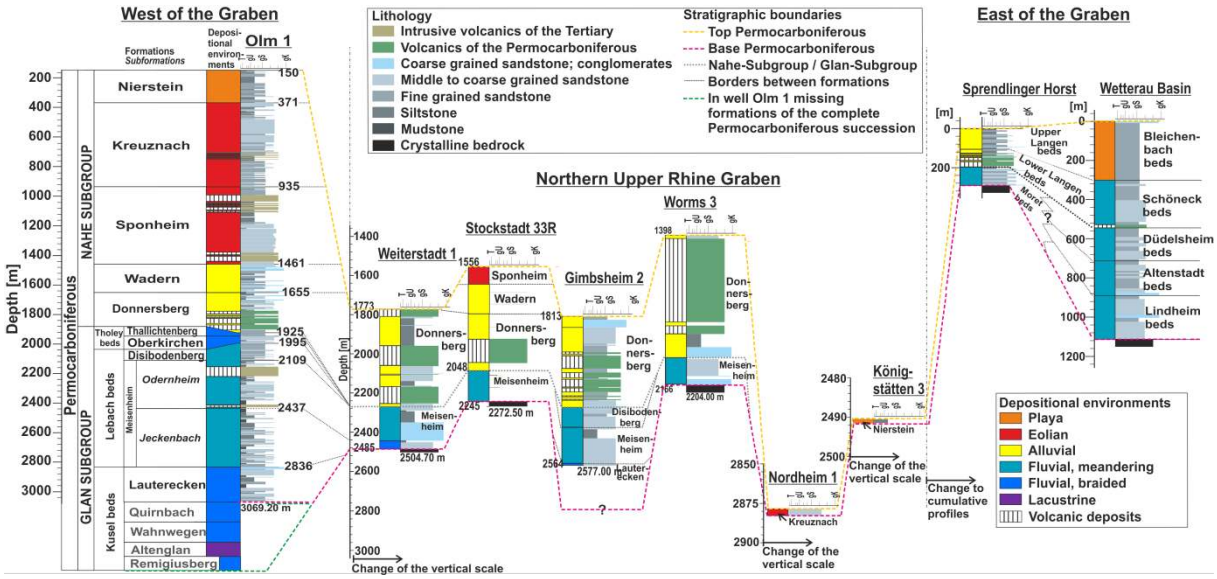

Fig. 2. Correlation of the lithostratigraphic units in consideration of the depositional environments based on deep exploration wells in the northern Upper Rhine Graben (Weiterstadt 1, Stockstadt 33R, Gimbsheim 2, Worms 3, Nordheim 1, Königstätten 3) as well as west of the graben (Olm 1), and compiled profiles of wells and outcrop areas of the Sprendlinger Horst and the Wetterau Basin east of the graben. For location of wells and compiled profiles see figure 1. Lithostratigraphic units after Lützner and Kowalczyk (2012), Saar Nahe Basin after Schäfer (2005), Upper Rhine Graben after Becker et al. (2012), Sprendlinger Horst after Marell (1989) and Müller (1996), Wetterau Basin after Kowalczyk (2001).

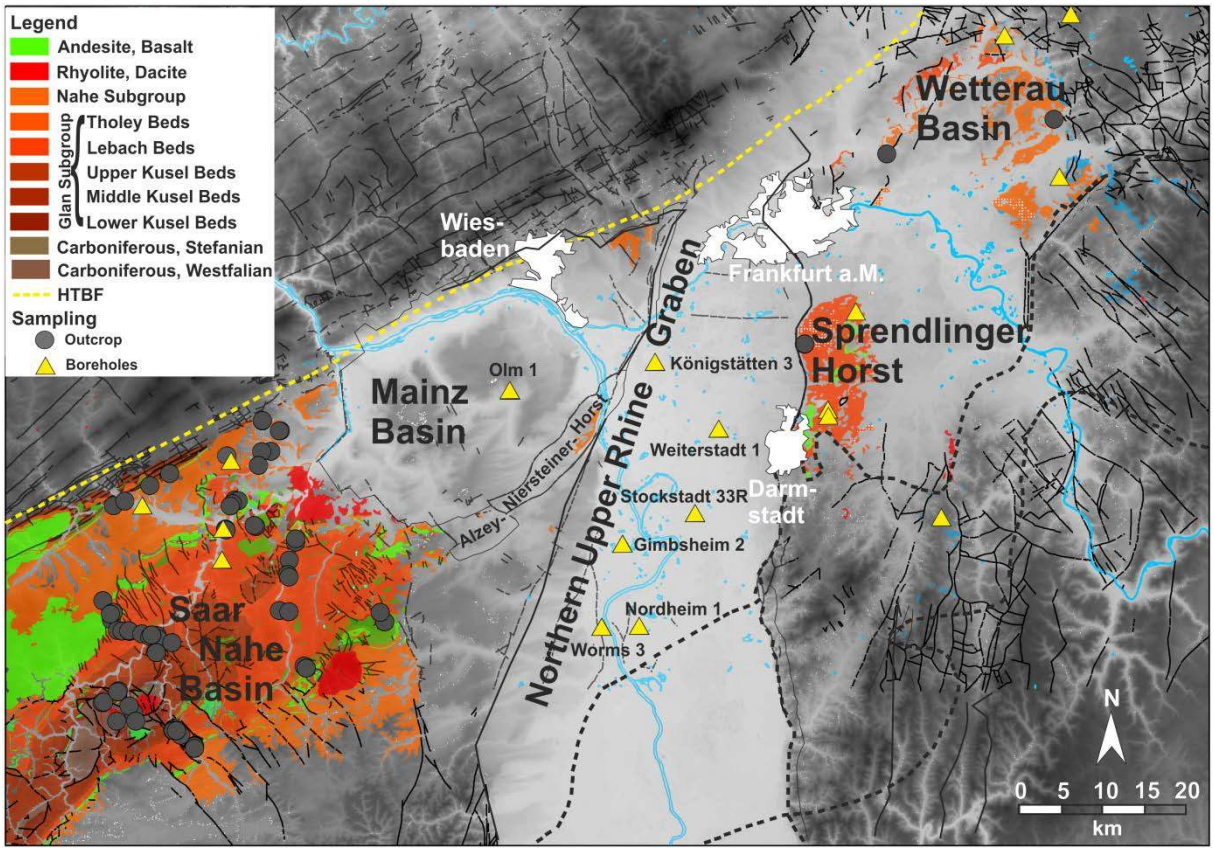

Fig. 3. Geological overview map of the outcrop analogue study areas west and east of the northern Upper Rhine Graben and locations of sampled outcrops (grey dots) and drill cores from shallow and deep wells (yellow triangles). Geological map based on GÜK 200, LGB-RLP; margins of the Permocarboniferous basin (yellow and black dashed lines) after Müller (1996). HTBF – Hunsrück Taunus Boundary Fault (yellow dashed line).

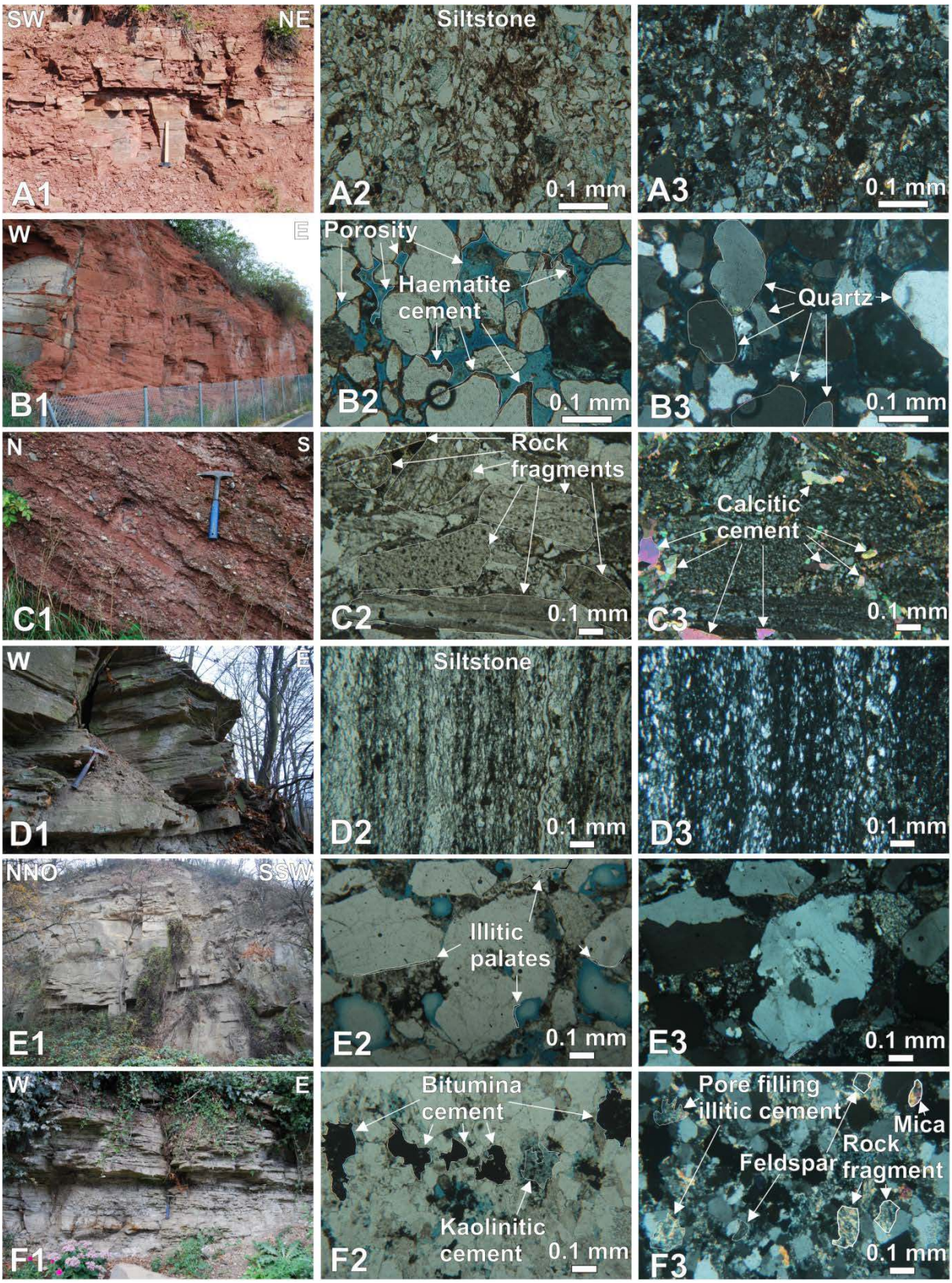

Fig. 4. Overview of outcrops of different depositional environments (1) and thin sections of samples taken from these outcrops in normal light (2) and under polarized light (3) with their petrographic characteristics. A) playa, B) eolian, C) alluvial, D) lacustrine, E) fluvial braided, F) fluvial meandering.

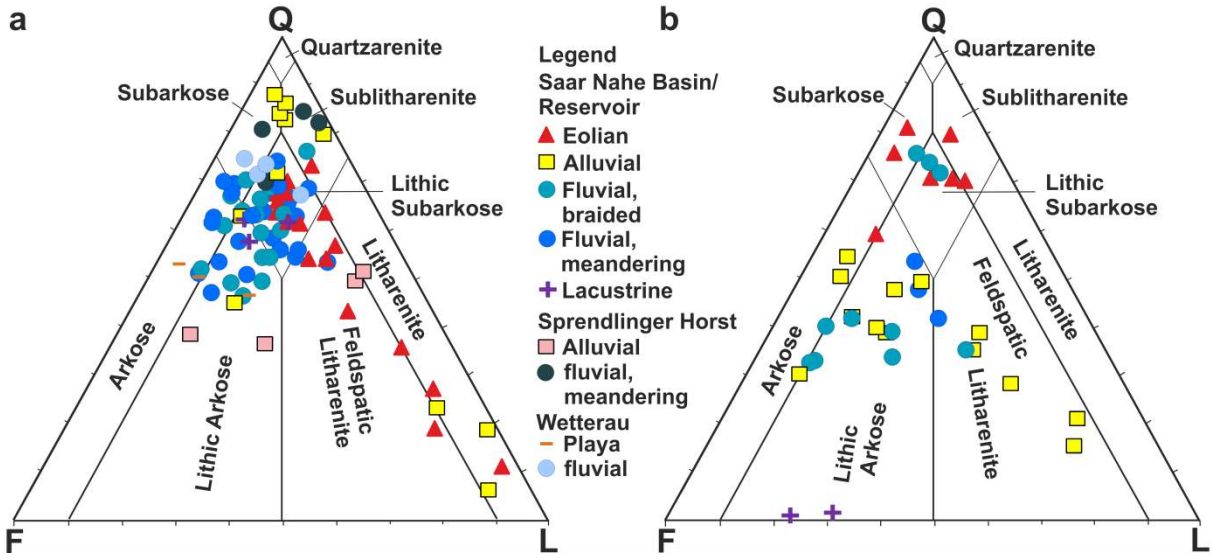

Fig. 5. Triangular QFL diagram showing the composition of the studied sandstones according to the Pettijohn (1975) classification scheme, a) outcrops sampled in the Saar Nahe Basin, Sprendlinger Horst and Wetterau Basin, and b) reservoir sampled in the northern Upper Rhine Graben.

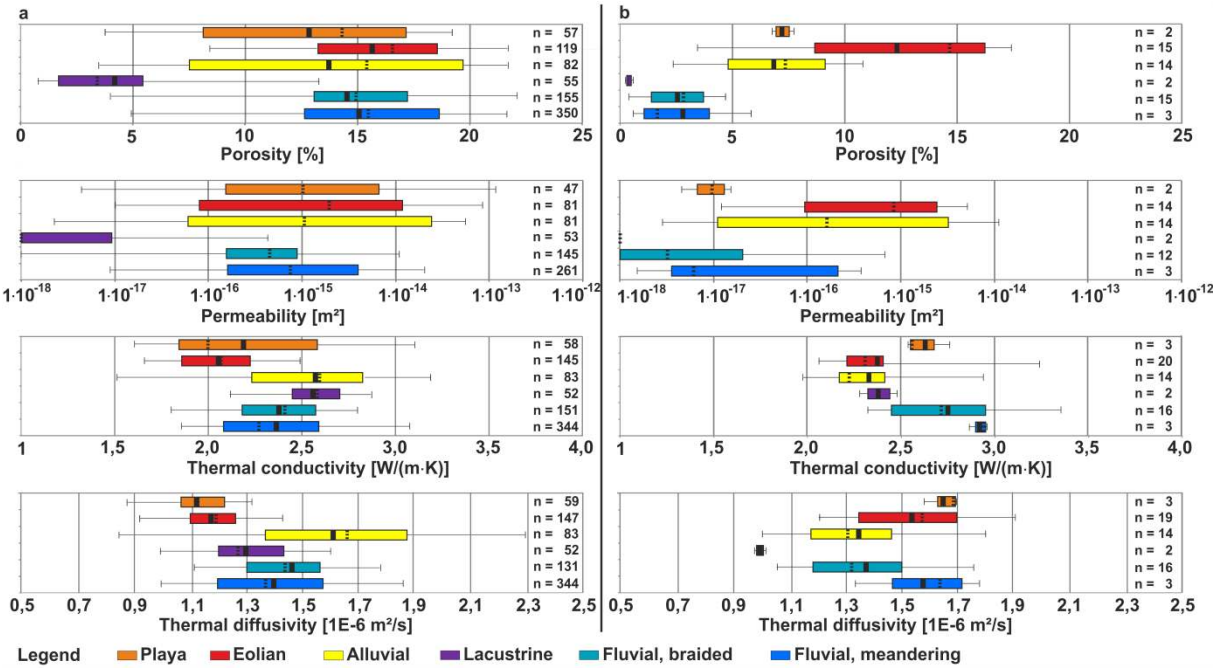

Fig. 6. Porosity, permeability and thermal conductivity box plot diagrams of a) outcrop samples from the Saar Nahe Basin, Sprendlinger Horst and Wetterau Basin and b) samples taken from reservoir depth from the northern Upper Rhine Graben, grouped according to the depositional environments. Porosities of outcrop samples are considerably higher for all depositional environments compared to the values of the reservoir samples, resulting in a significant increase of thermal conductivity and thermal diffusivity compared to the outcrop samples.

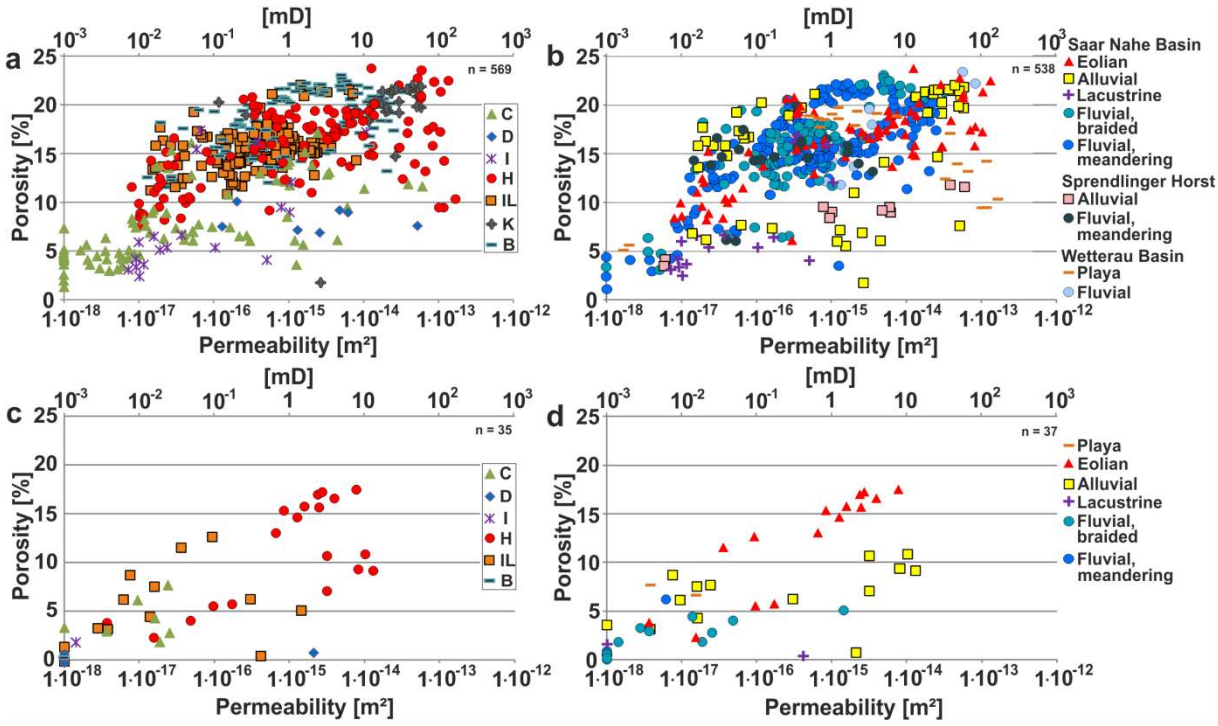

Fig. 7. Permeability-porosity plots grouped according to a) cementation types of outcrop samples, b) depositional environments of outcrop samples, c) cementation types of samples taken from reservoir depth and d) depositional environments of samples taken from reservoir depth. The general correlation of porosity and permeability follows the relationship described by Pape et al. (1999) for comparable settings of the Permocarboniferous of the Southern Permian Basin (Northern Germany). Abbreviations used: B – B-type sandstone, C – C-type sandstone, D – D-type sandstone, H – H-type sandstone, I – I-type sandstone, IL – IL-type sandstone, K – K-type sandstone.

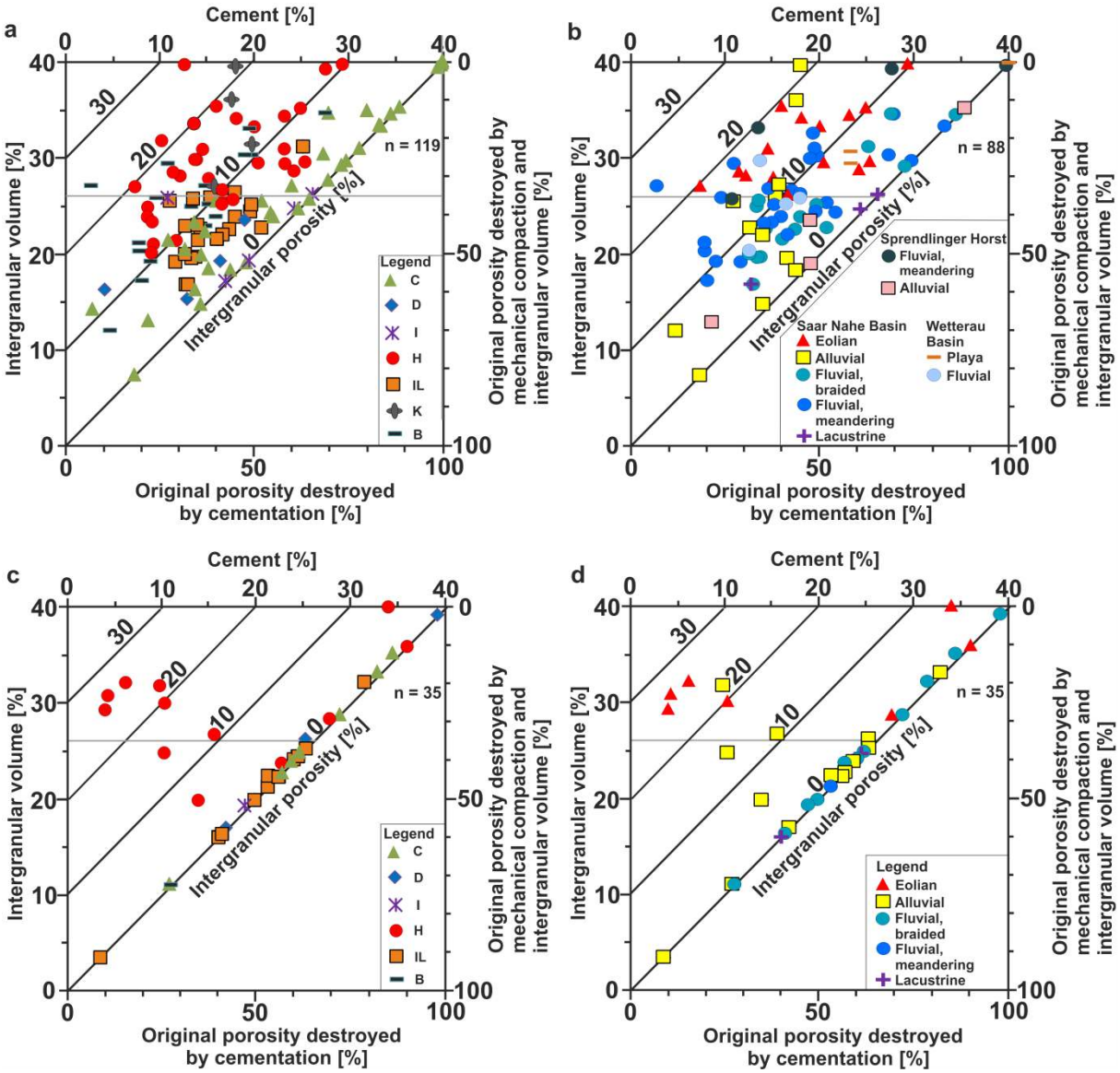

Fig. 8. Compaction diagram after Houseknecht (1988) grouped according to a) cementation types of outcrop samples, b) depositional environments of outcrop samples, c) cementation types of samples taken from reservoir depth, and d) depositional environments of samples taken from reservoir depth. Abbreviations used: B – B-type sandstone, C – C-type sandstone, D – D-type sandstone, H – H-type sandstone, I – I-type sandstone, IL – IL-type sandstone, K – K-type sandstone.

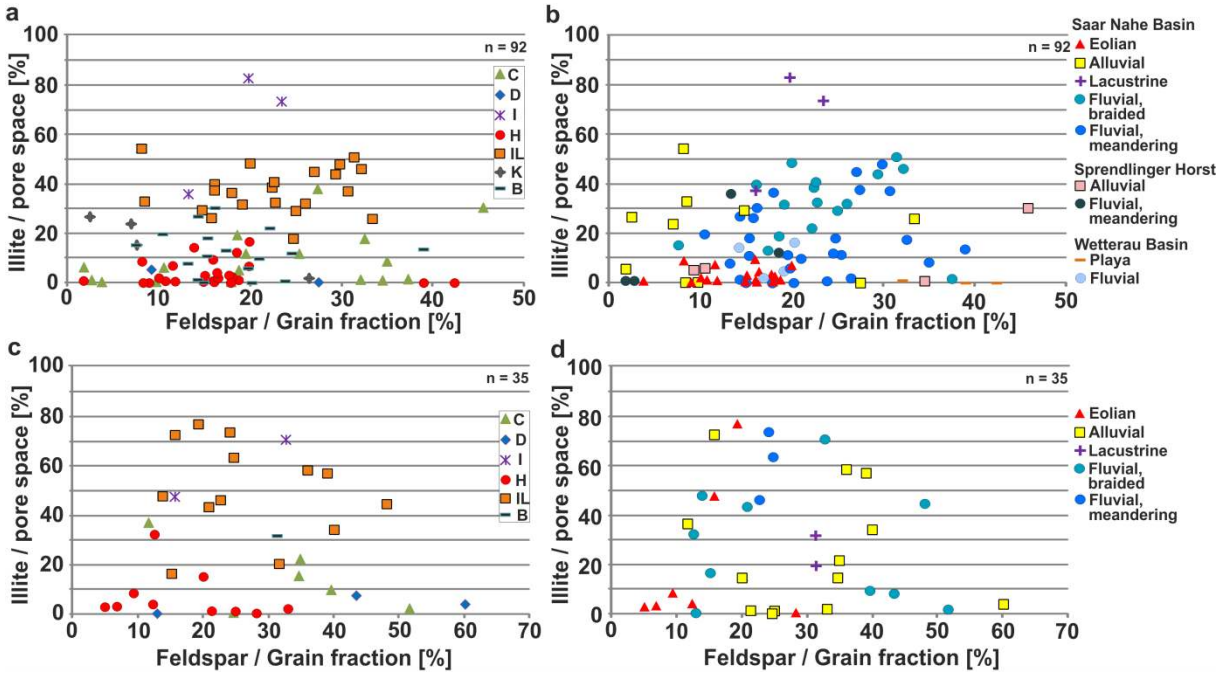

Fig. 9. Feldspar-illite diagram showing sandstone samples grouped according to a) cementation types of outcrop samples, b) depositional environments of outcrop samples, c) cementation types of samples taken from reservoir depth and d) depositional environments of samples taken from reservoir depth. Abbreviations used: B – B-type sandstone, C – C-type sandstone, D – D-type sandstone, H – H-type sandstone, I – I-type sandstone, IL – IL-type sandstone, K – K-type sandstone.

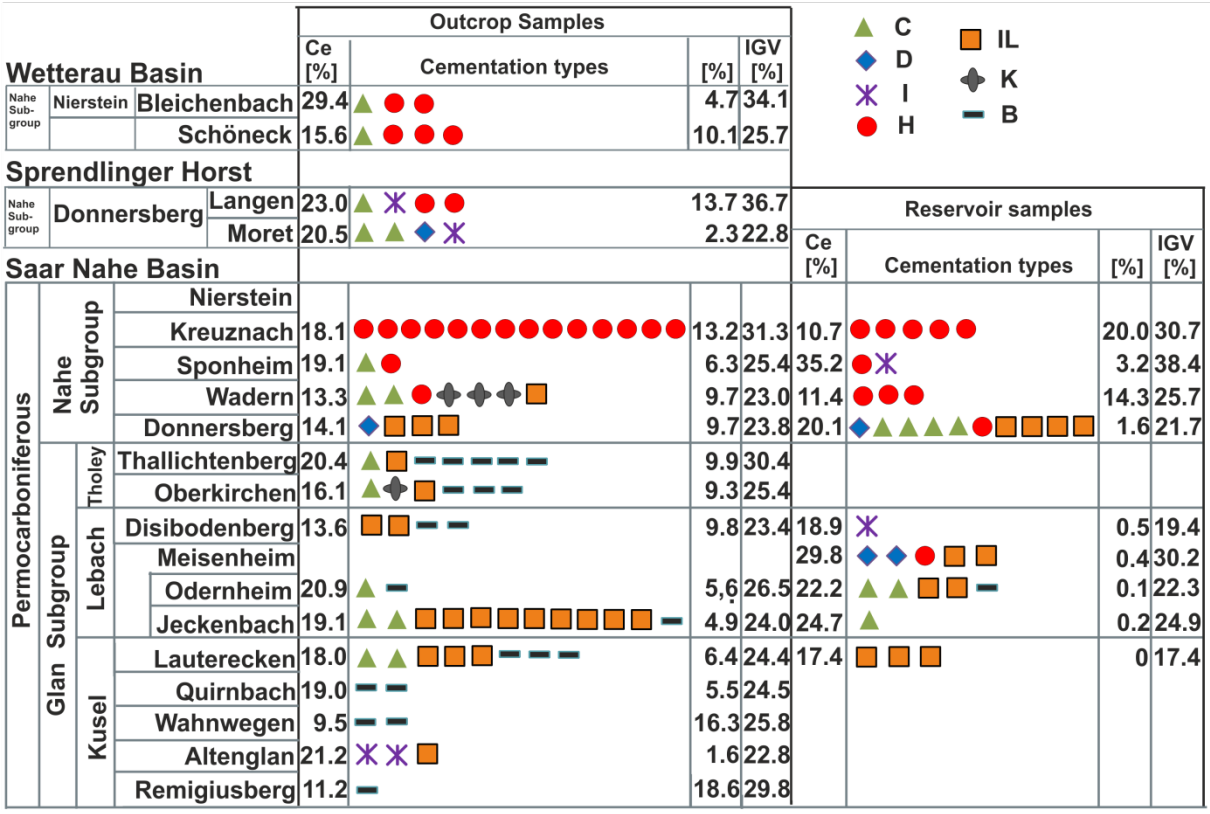

Fig. 10. Cementation types of outcrop samples of the Saar Nahe Basin, Sprendlinger Horst and Wetterau Basin and reservoir samples grouped according to the stratigraphic units of the Permocarboniferous. For each formation, the mean content of cement (Ce), porosity and IGV is listed. Abbreviations used: B – B-type sandstone, C – C-type sandstone, D – D-type sandstone, H – H-type sandstone, I – I-type sandstone, IL – IL-type sandstone, K – K-type sandstone.

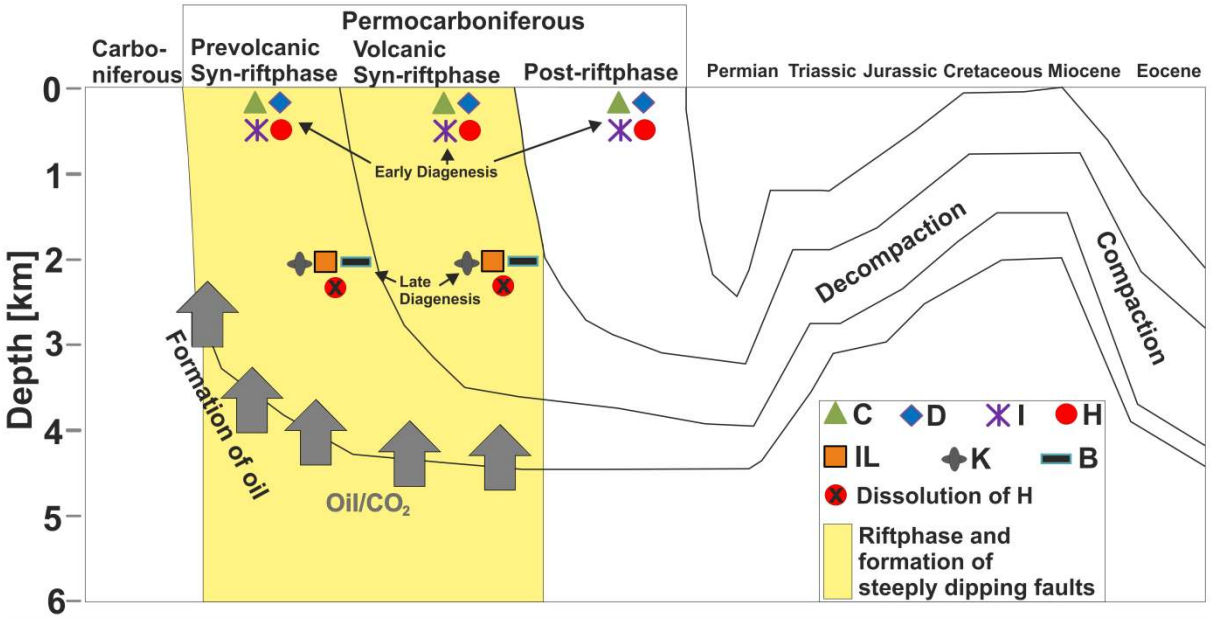

Fig. 11. Diagenesis diagram for the Permocarboniferous for the northern Upper Rhine Graben showing that the formation of the C- and D-type occurred before the formation of the I- and H-type. The rise of oil and CO_2-rich fluids from Carboniferous source rocks and dissolution of the H-type were bound to the rift phase and the formation of extension-related faults. The absence of IL-, K- and B-type sandstones in the post-rift phase is interpreted as reflecting the absence of newly formed extension-related faults which led to the preservation of the H-type and the best reservoir conditions in sandstones deposited in the post-rift phase after the decompaction due to erosion from the Permian to the Cretaceous (Henk, 1992), and the compaction due to the subsidence of the Upper Rhine Graben in the Miocene.